ELSEVIER

Tectonophysics 255 (1996) 243–268

TECTONOPHYSICS

Kinematics of convergence, deformation and stress distribution in the Taiwan collision area: 2-D finite-element numerical modelling

Jyr-Ching Hu [a], Jacques Angelier [a], Jian-Cheng Lee [a], Hao-Tsu Chu [b], Daniel Byrne [c]

[a] *Tectonique Quantitative, URA 1315, CNRS, Université P. et M. Curie, 4 place Jussieu, T26, E-1, 75252 Paris Cedex 05, France*
[b] *Central Geological Survey, PO Box 968, Taipei, Taiwan*
[c] *Instituto de Geofisica, UNAM, Ciudad Universitaria, 04510 México, D.F., Mexico*

Received 17 January 1994; accepted 29 September 1995

Abstract

Using a 2-D plane stress finite-element model with elastic and elasto-plastic rheologies, appropriate for deformation within the brittle upper crust, we analyse the relationship between kinematics of convergence, deformation and stress distribution in the present Taiwan collision occurring between the Ryukyu and Luzon subduction zones.

The distribution of stress trends calculated in our models is compared with a synthetic map of actual stress trajectories based on the most recent data available in the collision zone. These data combine present-day sources (from borehole breakouts and earthquake focal mechanism) with the reconstruction of Quaternary palaeostress (from fault slip data analyses), resulting in a complete map of compressional stress trajectories which is used to constrain our models.

We show that the distribution of stress trajectories in the active Taiwan collision is principally controlled by: (1) the geometric configuration of the boundary between Eurasia and the Philippine Sea plate; (2) the shape and rheological properties of major structural units; (3) the direction of convergence of the Philippine Sea plate relative to Eurasia; and (4) the influence of the opening of the Okinawa Trough.

The study of a two-dimensional elastic and elasto-plastic finite-element modelling of the subduction–collision in and around Taiwan allows us to estimate the influences of these different parameters in the stress pattern. Taking into account both the simplifying assumptions of the numerical modelling and the angular uncertainties of field determinations, the fit between the calculated stress pattern of the finite-element model and that determined based on the geometrical synthesis of field analyses is rather good in general, indicating that our model is valid to first approximation. Misfits remain minor and can be explained by data uncertainties and simplifying modelling assumptions (for instance, the shape of the corner of the collision zone is critical but is not accurately known; also limited decoupling in the Longitudinal Valley collision zone was not considered in our models although it certainly plays a role).

Some interesting features of our model are: (1) the greater influence of the shape of the collision zone in comparison with that of the direction of convergence; (2) the requirement for a trench retreat related to suction force in the Ryukyu Arc; and (3) the crucial role of the interaction between Okinawa Trough opening and collision at the sharp northwestern corner of the Philippine Sea plate including its influence on the geological evolution of northeastern Taiwan.

SSDI 0040-1951(95)00140-9

1. Introduction

Taiwan provides a good example for understanding the behaviour of a collision zone with active crustal shortening, the Taiwan orogen. This collision zone where mechanical coupling occurs is located along the convergent boundary between the Philippine Sea plate and Eurasia. Two subduction zones with decoupling, the Ryukyu and Manila arc-and-trench systems, are present along this boundary, east and south of Taiwan, respectively (Fig. 1).

Numerous recent studies have contributed to a better knowledge of the tectonic evolution of the Taiwan collision, in terms of general geology and mountain building processes (Hsu, 1956; Biq, 1966; Yen, 1973; Suppe, 1980, 1981, 1984; Ho, 1982, 1986, 1988; Chen et al., 1983; Liou and Ernst, 1984; Jahn et al., 1986; Pelletier and Stephan, 1986; Teng, 1990; Lu and Hsü, 1992; Delcaillau et al., 1993). The seismicity of the area was also described in detail (Tsai et al., 1977; Wu, 1978; Tsai, 1986; Roecker et al., 1987; Yeh et al., 1991), as well as the compressional structure and tectonic mechanisms in this collision zone (Barrier, 1985, 1986; Barrier and Angelier, 1986; Angelier et al., 1986, 1990; Lee, 1986; Chu, 1990; Lee et al., 1991; Lacombe et al., 1993).

Although the general link between the compression in Taiwan and the plate convergence is obvious (Fig. 1a), the quantitative relationships in terms of displacement and deformation trends are difficult to recognize, due to the complex shape of the plate boundary and the obliquity of relative motion. In more detail, two interesting phenomena in terms of the regional tectonic stress state are the clockwise deviation of stress trajectories in northern Taiwan and the presence of extensional tectonics in the Okinawa Trough area. In 1986, based on an earlier structural and tectonic knowledge of the collision and subduction zones of the Taiwan area, and taking into account the independent information on the kinematics of the Philippine Sea plate relative to Eurasia (Seno, 1977; Minster and Jordan, 1979; Ranken et al., 1984; Huchon, 1986), several 2-D

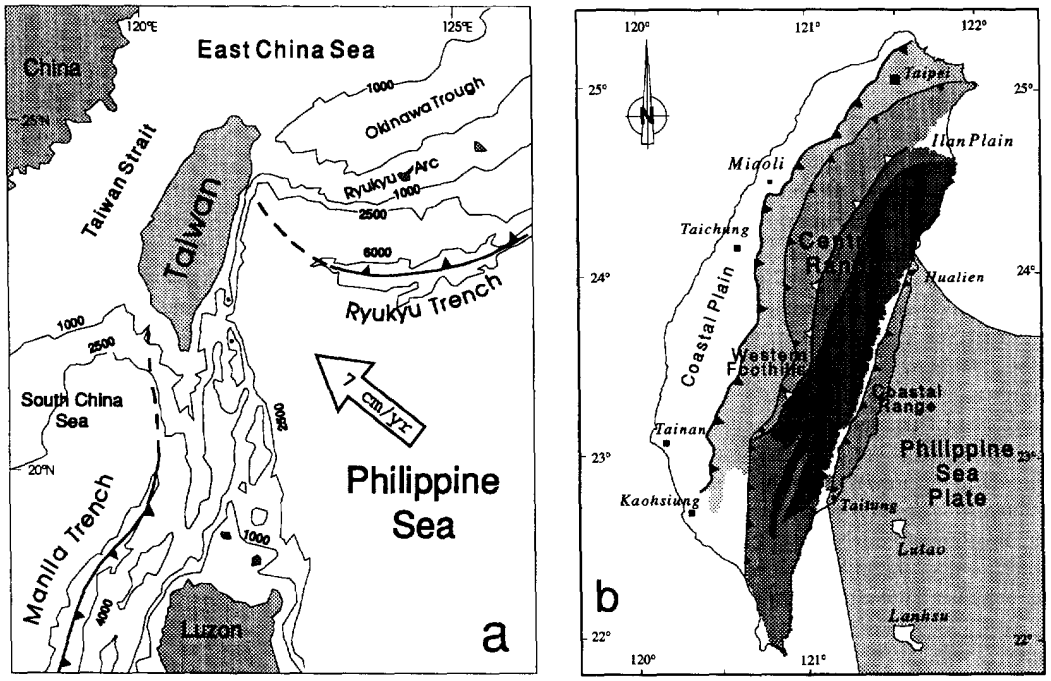

Fig. 1. Location map and main tectonic units in Taiwan. (a) Geodynamic framework: isobaths in metres; large open arrow show the present direction of convergence (Philippine Sea plate relative to Eurasia); thick lines indicate subduction (triangles on overriding side). (b) Tectonic framework and main structural units: major thrust faults with triangles on the upthrust side (*L.V.* = Longitudinal Valley).

finite-element models with different rheologies and boundary conditions were proposed. Huchon et al. (1986) proposed a 2-D viscous finite-element model for simulating a rigid body (the Luzon Arc) indenting into a rigid–plastic material (the Chinese continental margin). Lee (1986) proposed a 2-D finite-element model of plane strain with the joint element in order to partially simulate the effects of mechanical decoupling along the active Longitudinal Valley Fault, the Lishan Fault and the Okinawa Trough. Both these models successfully produced a fan-shaped compressional stress pattern radiating from the collision zone, the trends of stress trajectories being sensitive to the direction of the collision. Viallon et al. (1986) proposed a 2-D finite-element model with an elasto-plastic behaviour, and showed that the opening of the Okinawa basin behind the Ryukyu Trench can be explained by a retreating trench model with lateral anchoring due to the collision in Taiwan. They highlighted the role of a suction force applied to the edge of the overriding plate, due to subduction of the oceanic lithosphere of the Philippine Sea basin.

In this paper, we aim at presenting a more general model of the Taiwan plate convergence area, integrating both the compressional geodynamics of the collision zone and the edge effects related to subduction processes, especially in the neighbouring Ryukyu arc-and-trench system. We take into account the results of recent kinematic analyses (Seno et al., 1987, 1993; DeMets et al., 1990; Table 1), as well as the results of the most recent palaeostress analyses in Taiwan (e.g., Angelier et al., 1990; Chu, 1990, 1993; Lacombe et al., 1993). We thus present an overall tectonic model for both the Taiwan orogen and the neighbouring arc-and-trench systems, shown in Fig. 1. This model is based on finite-element numerical modelling with appropriate rheologies and boundary conditions. We use a 2-D plane stress model, which allows us to reproduce the complex distribution of major structural units and tectonic zones in the area. We adopt elastic and elasto-plastic rheologies, appropriate for deformation within the brittle upper crust. We thus attempt to explain the relationships between stress distribution and convergent kinematics in the whole subduction and collision zones in and around Taiwan during the Plio–Pleistocene.

2. Tectonic setting of Taiwan

2.1. Structure of the Taiwan collision zone

The island of Taiwan is located along a segment of the convergent boundary between the Philippine Sea plate and Eurasia, where collision as well as subduction processes occur (Fig. 1a). The Philippine Sea plate is subducting beneath the Eurasian plate at the Ryukyu Trench and overriding the crust of the South China Sea at the Manila Trench (Fig. 2a). The SE-facing Ryukyu arc-and-trench system extends from southern Kyushu (Japan) to the east of Taiwan, where it trends W–E at 23–24°N east off Hualien. This subduction zone is associated with the back-arc spreading of the Okinawa Trough, which ends to the west in the Ilan Plain of northeastern Taiwan (Fig. 1), where extensional seismic activity occurs (Tsai, 1986). In contrast, the W-facing Luzon–Manila arc-and-trench system extends from the Philippines to about 22°N near Kaohsiung (Fig. 1), where it merges into the mountain ranges of Taiwan.

As Fig. 1b shows, Taiwan can be divided into two major tectonic provinces separated by the active Longitudinal Valley Fault (Ho, 1986, 1988). The narrow eastern province, including the Coastal Range and the two islands of Lutao and Lanhsu, is a remnant Neogene island arc usually interpreted as the leading edge of the Philippine Sea plate, that is

Table 1
Philippine–Eurasia relative plate motion estimates off eastern Taiwan at 23°N 122°E

Ref.	Rotation poles			Linear velocity, 23°N 127°E	
	Lat. (N°)	Long. (°E)	ω (°/Ma)	Velocity (mm/yr)	Azimuth (°)
1.	45.50	150.62	1.200	70.7	309
2.	48.20	157.00	1.090	73.7	309
3.	47.30	154.40	1.060	68.2	310
4.	38.80	142.00	1.950	83.8	314
5.	37.00	141.00	1.600	65.3	315
6.	48.26	162.45	1.227	105.0	321

Geographic coordinates of Euler Poles (latitudes, longitudes) and their angular velocities (ω) from different models. References: 1 = Seno, 1977; 2 = Seno et al., 1993; 3 = Seno et al., 1987, and DeMets et al., 1990; 4 = Huchon, 1986; 5 = Ranken et al., 1984; 6 = Minster and Jordan, 1979.

the northern extension of the Luzon Arc (Figs. 1 and 2a). The large western province, which includes most of Taiwan, is usually divided into several stratigraphic and structural units, based on rock types and degrees of metamorphism. These units are generally bounded by major faults and thrusts. The main units

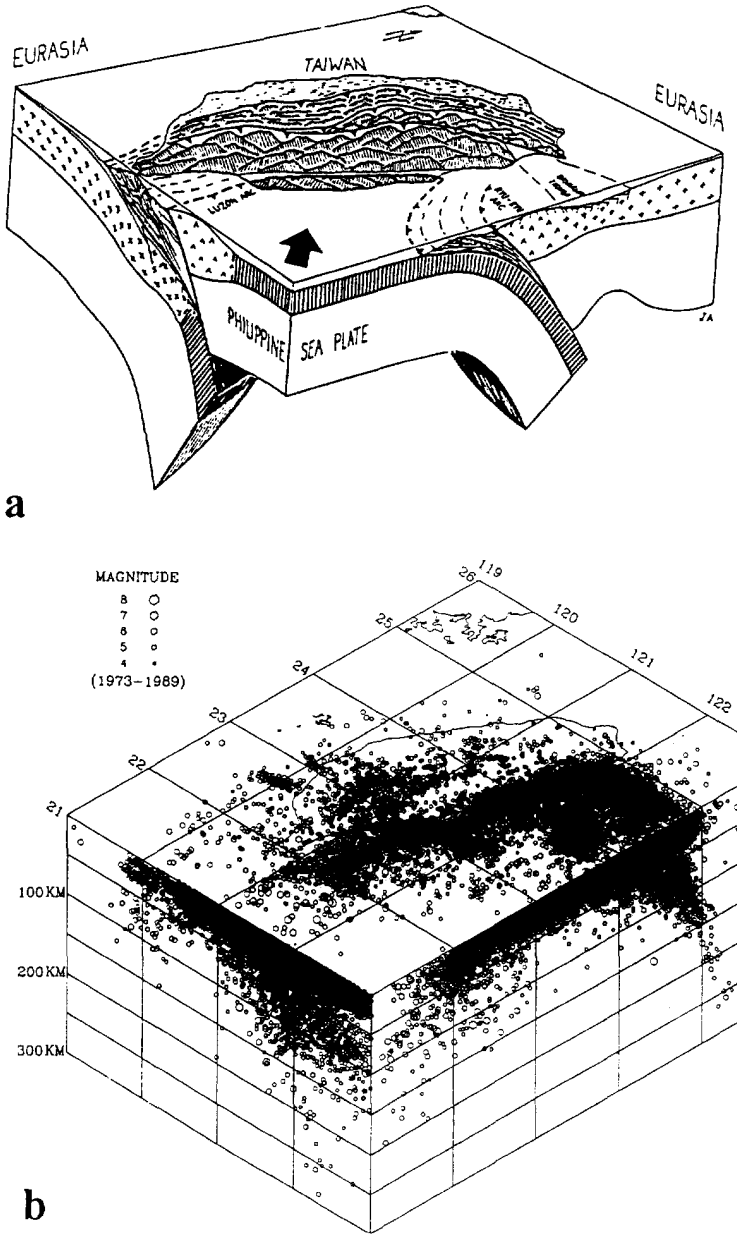

Fig. 2. 3-D structure of the Taiwan collision zone. (a) Lithospheric structure in and around Taiwan from Angelier (1986), main thrusts as thick lines, with triangles on the upthrust side; in sections: oceanic crust hatchured, continental crust with pattern of crosses, island-arc crust with pattern of overturned 'v' and lithospheric mantle left white. (b) Earthquake distribution, from Yeh et al. (1991): map of epicentres and projections of hypocentres in E–W and N–S sections, for the most reliably located earthquakes by the Taiwan Telemetered Seismographic Network (1973–1989).

are, from east to west: (1) the Central Range; (2) the Western Foothills; and (3) the Coastal Plain (Fig. 1b). The Central Range of Taiwan is characterized by the presence of Tertiary metamorphism, in contrast with the adjacent non-metamorphic fold-and-thrust belt of the Western Foothills (Chen and Chu, 1983; Ho, 1986). The pre-Tertiary basement, which has been affected by Neogene greenschist facies as well as by higher grades of polyphase Mesozoic–Cenozoic metamorphism, crops out in the eastern flank of the Central Range. The axial ridges and the western flank constitute the Slate Belt. In the Western Foothills, Miocene, Pliocene and Early Pleistocene shallow marine to shelf clastics sediments thicken from north to south and east to west. These sediments are affected by WNW-vergent folds and low-angle thrust faults. The Coastal Plain is composed of Quaternary alluvial deposits derived from the Central Range and the Western Foothills.

It is widely considered that the western tip of

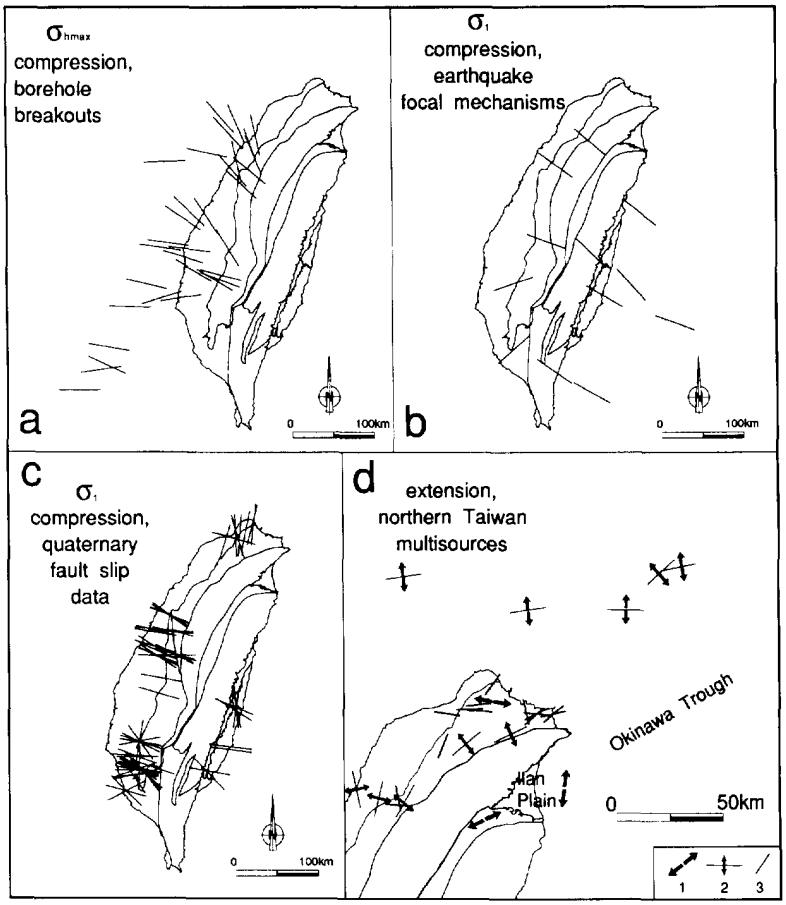

Fig. 3. Present-day stress distribution in Taiwan. (a) Inferred maximum horizontal stress orientation (σ_{hmax}) indicated by borehole breakouts (after Suppe, 1984). (b) Regional synthesis of maximum compressional stress orientations (σ_1), for twelve groups of earthquake focal mechanism data (after Yeh et al., 1991). (c) Paleostresses related to Quaternary collision, as reconstructed in Quaternary formation solely; maximum compressional stress orientations (σ_1), based on stress tensor reconstructions from local sets of brittle tectonic data (Barrier and Angelier, 1986; Angelier et al., 1986, 1990; Chu, 1990, 1993; Lacombe et al., 1993). (d) Distribution of extensional stress in northern Taiwan, from various sources (the same as for (a), (b), (c)): *1* = focal mechanism data (couples of arrows indicate σ_3 trend); *2* = borehole breakout data (arrows for σ_{hmin}, bar for σ_{hmax}); *3* = Quaternary fault slip data (bars indicate σ_3).

Okinawa Trough is the Ilan Plain of northeastern Taiwan (Fig. 1), based on bathymetric trends and distribution of earthquakes (Tsai et al., 1977; Tsai, 1986; Ho, 1986; Yeh et al., 1989, 1991). According to Letouzey and Kimura (1985, 1986), the Okinawa marginal basin opened due to crustal extension behind the Ryukyu Arc in the Asian continent since about 2 Ma ago (Fig. 2a).

2.2. Distribution of earthquakes

The seismic activity in the Taiwan area (Fig. 2b) is illustrated by the distribution of epicentres and the projection of centres of more reliably located earthquakes during 1973–1989 by the TTSN (Taiwan Telemetered Seismographic Network). Tsai et al. (1977) and Tsai (1986) recognized three major seismic zones: (1) the northern zone, which approximately follows the meridian 121.5°E between 24.0°N and 23.5°N, marks the western edge of the subducted Philippine Sea plate; a Benioff seismic zone dipping about 45–50° to the north to a depth of about 140 km, beneath northeastern Taiwan; many earthquakes in this seismic zone are located in the overlying continental crust; (2) the eastern seismic zone includes the Longitudinal Valley, the Coastal Range and the adjacent offshore area to the east; it is bounded on the west side by a well-defined surface dipping 50–55° toward the east from the surface (in the Longitudinal Valley) down to a depth of about 50 km (beneath the eastern coast of Taiwan); (3) the western seismic zone includes most of the Hsüehshan Range and of the Western Foothills; most earthquakes in this zone are located in the upper crust. The distribution of earthquakes in southern Taiwan revealed that an east-dipping Benioff zone may exist, as a northern extension of the Manila subduction zone (Tsai, 1986; Roecker et al., 1987). This earthquake distribution (Fig. 2b) corresponds to the complex pattern of lithospheric slabs beneath Taiwan (Fig. 2a).

3. Stress distribution in Taiwan

3.1. Present-day stress distribution

Because we first consider the present-day kinematics of the Philippine Sea plate, the fit of our models must be done by using all stress data which reflect the most recent step in the geodynamic evolution of the collision zone. As a consequence, it is necessary to examine the data on present-day and recent stresses in and around Taiwan. The present-day distribution of stress in Taiwan was obtained from two principal sources of data (Fig. 3a,b): the borehole breakouts analysed by Suppe et al. (1985), and the groups of earthquakes focal mechanisms analysed by Yeh et al. (1991).

The map of maximum compressional stress trends obtained from borehole breakout data describes the stress state in the uppermost crust of Taiwan (Suppe et al., 1985), in terms of trends of maximum compressional horizontal stress, σ_{hmax}, revealed by hydraulic fracturing experiments in Taiwan boreholes (Fig. 3a). Note that in the collision zone σ_{hmax} generally corresponds to the maximum compressional stress axis, σ_1, while an other principal stress axis, σ_2 or σ_3, is nearly vertical (strike-slip faulting or reverse faulting mode, respectively). In most regions of the island, σ_1 axes are nearly horizontal (Fig. 3a); recent structures are clearly compressional, as shown by analyses of recent and active faults. In few regions of Taiwan, however, σ_{hmax} corresponds to the intermediate principal stress axis, σ_2, while σ_1 is vertical (normal faulting mode, indicating extensional tectonics): this is typically the case in northeastern Taiwan, where extensional tectonism occurs in and around the Ilan Plain (Fig. 3d).

Yeh et al. (1991), using the stress tensor analysis developed by Angelier (1979, 1984) and grouping data on earthquakes focal mechanisms from 1972 to 1986 in several regions, reconstructed the different stress regimes in the crust of the Taiwan area. Whereas borehole breakout data simply indicate local σ_{hmax} trends (Fig. 3a), analyses of groups of focal mechanisms allow determination of stress tensors, indicating the trends and plunges of the three principal stress axes, σ_1, σ_2 and σ_3. As a result, the stress regimes are determined unambiguously in three dimensions. In Fig. 3b, the trends of maximum compressional stress axes are shown only where the corresponding tectonic regime is clearly compressional (i.e., a shallow plunge of σ_1 and a nearly vertical σ_2 or σ_3 axis, indicating strike-slip or reverse faulting modes, respectively). The results corresponding to extensional activity, omitted in Fig.

3b, are shown in Fig. 3d. Shallow-plunging minimum principal stress axes σ_3, which trend approximately N–S (Yeh et al., 1991), were reconstructed in this region of low seismic velocities (Fig. 3d). As a result, following Tsai (1986), the Ilan Plain area should be considered as a western onland extension of the Okinawa Trough back-arc basin (Figs. 1a and 2a).

In summary, all determinations of present-day stress indicated that the regional stress in the Taiwan region is dominated by NE–SW compression (Figs. 3a,b), due to collision between Eurasia and the Philippine Sea plate. In addition, active extension occurs in northeastern Taiwan (Fig. 3d), at the western tip of, and mostly perpendicular to, the W–E-trending Okinawa Trough.

3.2. *Palaeostresses related to Plio–Quaternary collision*

The distribution of Late Cenozoic palaeostresses in Taiwan has been studied in detail based on fault slip data analyses (Barrier and Angelier, 1986; Angelier et al., 1986, 1990; Lee, 1986; Chu, 1990). These studies revealed that the compressional events of the Plio–Pleistocene collision between the Luzon Arc (belonging to the Philippine Sea plate) and the Chinese continental margin (belonging to Eurasia) are widespread in the whole Taiwan area; they also indicated that most trends of compression are ESE–WNW, SE–NW and SSE–NNW (Fig. 3c).

These Plio–Quaternary patterns of compressional stress related to collision cannot be considered as a whole because it has been demonstrated that significant changes have occurred over time. Especially the late Plio–Pleistocene records of compressional palaeostresses could be separated into two principal tectonic events, as proposed by Angelier et al. (1986). Further detailed analyses, especially in the Hsüehshan Range in northern Taiwan (Angelier et al., 1990), revealed increasing complexity of the palaeostress compressional regimes successively recorded in Taiwan since the Late Miocene (Chu, 1990). However, fan-shaped patterns of palaeostress trajectories were recognized (Angelier et al., 1986, 1990, 1994; Chu, 1990). This particular distribution of palaeostress in Taiwan probably reflects the oblique indentation of the Luzon Arc into the Eurasian continental margin.

Due to the variation of the stress field with time, it would not be appropriate to include all Late Cenozoic palaeostress determinations in our first reconstruction, primarily based on present-day kinematics.

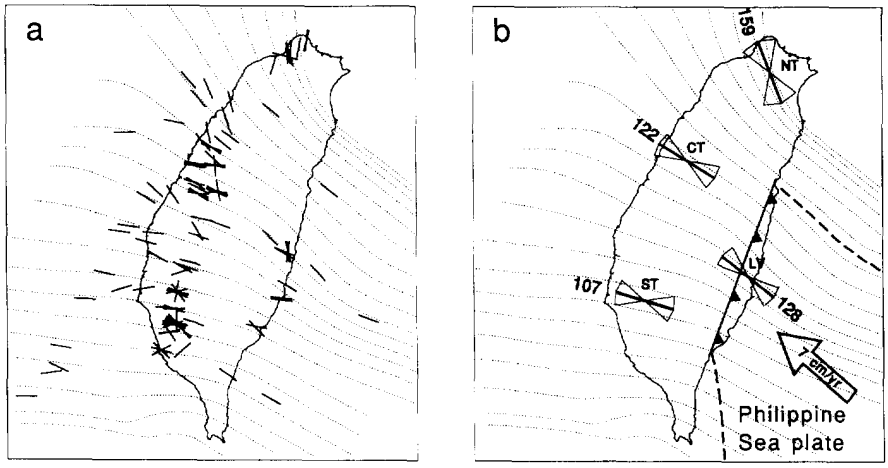

Fig. 4. The distribution of Quaternary and present-day stresses throughout Taiwan: a synthesis. (a) Summary of the observed maximum stress directions (from Fig. 3), and corresponding calculated trajectories of σ_1, shown as thin dashed lines. (b) Main stress field associated with the Quaternary collision (same σ_1 trajectories as in (a)), with σ_1 trends and their standard deviations at four reference sites in Taiwan. Plate boundary added as thick line with triangles on the upthrust side: *NT, CT, LV, ST*, reference sites (northern Taiwan, central Taiwan, Longitudinal Valley, southern Taiwan). Vector of relative plate motion added (see also Fig. 1). Azimuths and standard deviations listed in Table 2.

The separation of events is a complex problem, discussed in detail elsewhere (Angelier et al., 1986, 1990; Chu, 1990). As the simplest solution, we consider all the palaeostress results obtained in the Quaternary formations (Fig. 3c) and we neglect the results obtained in older terranes. Reconstructions of stress trajectories independently carried out with present-day data (Fig. 3a,b) and Quaternary ones (Fig. 3c) are not described in detail herein, because the differences are not significant within the range of angular uncertainties in stress determinations, so that all these data can be combined in a single map of compressional trajectories (Fig. 4).

3.3. The map of Quaternary stress / palaeostress distribution

Because we first aim at presenting a finite-element model of the most recent steps in the Taiwan collision, we combine the three sources of stress data shown in Fig. 3a–c, in order to build the synthetic map of Fig. 4a. The only borehole breakout data absent in Fig. 3a correspond to extension in northernmost Taiwan (these data are shown in Fig. 3d), plus two data in southwestern Taiwan, which probably also correspond to local extension. Summarizing, in Fig. 4, we simply consider the major compressional stress field, trending NW–SE and related to collision.

Fig. 4a shows both the data retained from Fig. 3 (a, b, c) and the corresponding compressional stress trajectories (σ_1), for the most recent event of the collision (recent Pleistocene to Present). These trajectories were drawn using a smoothing procedure proposed by Lee and Angelier (1994) with the following sources of information: the stress tensors determined by fault-slip data in the Quaternary formations (Fig. 3c), the stress tensors reconstructed with earthquakes (Fig. 3b) and the borehole breakout data (Fig. 3a). The three sources of data play similar roles in the whole reconstruction of recent stress trajectories (Fig. 4), because we used different weighting factors: 1 for Quaternary palaeostress data, 2 for borehole breakout data and 5 for stress tensors reconstructed by focal mechanisms. In addition, in order to facilitate further discussion and comparisons, four representative localities (northern Taiwan, NT; central Taiwan, CT; southern Taiwan, ST; Longitudinal Valley, LV) have been chosen as control points (Fig. 4b and Table 2). The first three reference sites have been selected in the Western Foothills near the front of the mountain belt where tectonic data are abundant and stratigraphy dating easier. The fourth site corresponds to a major zone of deformation where active shortening occurs (Tsai, 1986; Yu and Liu, 1989) as well as Quaternary compression (Barrier and Angelier, 1986).

Table 2
Results of maximum stress trends σ_1 and their standard deviations for combining different sources of data (see Figs. 3 and 4) at four selected reference sites of Fig. 4b (azimuths in degrees)

Site	Lat. °N	Long. °N	σ_1 trend
NT	121°35′	24°57′	159 ± 26
CT	120°52′	24°12′	122 ± 22
LV	121°11′	23°06′	128 ± 20
ST	120°27′	22°52′	107 ± 28

The statistical variance of calculated compressional trends is first dependent on the uncertainties of local determinations, and second on the smoothing parameters adopted in trajectory calculations. The uncertainty on each local tensor determination depends on the number, accuracy and mechanical consistency of the fault slip data used. In the smoothing process, the disk of radius R represents the smoothing influence field and p is the power value of the weighting function (for details on weighting procedure, see Lee and Angelier, 1994). Fig. 4b was smoothed with the coefficients $R = 90$ km and $p = 2$; the standard deviations at the four reference points range from 20° to 28°. Table 2 and Fig. 4b show the azimuths and standard deviation of maximum compressional stress (σ_1). The average trends of σ_1 decrease from north (159° for northern Taiwan) to south (107° for southern Taiwan). Standard deviations are large due to dispersion of local data, because all determinations were taken into account: had local perturbations been taken into account and corrected, the deviations would have been smaller. Such perturbations and stress deviations commonly occur near large fault zones, and permutations between principal stress axes may even take place (in this case, σ_1 and σ_2). It seemed preferable, however, to use the complete set of tectonic data than to introduce an additional interpretation. We conclude

that the variation in compressional trends along the Taiwan mountain belt is significant (Fig. 4). Finally, Fig. 4b summarizes the major data used in fitting our models, which include the direction of plate convergence, the shape of the plate boundary and the distribution of recent compressional stress in the collision zone.

4. Finite-element modelling

4.1. The finite-element technique

The model used here is a two-dimensional model which includes a variety of subdomains with different material properties (Table 3), in order to represent the mechanical behaviour of different regions (Fig. 5). This configuration was chosen according to the regional structural framework of the area under investigation (Fig. 1). Numerous experiments were done, with different boundary conditions and rheologies. The stresses and displacements were calculated with a two-dimensional, plane-stress, finite-element technique developed by the 'Institut National de Recherche en Informatique et en Automatique' (George et al., 1986).

The matrix equation of the standard finite-element method for steady-state problems can be expressed in the following form:

$$[k]\{d\} = \{F\} \quad (1)$$

where $\{d\}$ is the matrix of nodal displacements, $\{F\}$ is the matrix of all nodal loads and $[k]$ is the sum of all the element stiffness matrixes. The problem consists of solving a system of linear equations. Once the nodal displacements are known, the stress components (σ_k) at the centroid of each element can be solved by a planar interpolation of the stress concentration across the element from the equation:

$$\{\sigma\} = [C][B]\{d\} \quad (2)$$

where $[C]$ is the constitution matrix and $[B]$ is the strain displacement. Our modelling thus uses the small strain approximation for the elastic model and assumes that continuous infinitesimal deformation occurs throughout the region studied. Due to the obvious limitations of the elastic model, we have also used an elasto-plastic model with the Von Mises criterion, which is more realistic and better accounts for the actual deformation of the mountain belt. With this elasto-plastic model, large deformations can be considered.

Table 3
Rheology and parameters used in the finite element modelling (compare with Fig. 5)

Subdomain	Young's modulus (GPa)	Poisson's ratio	Yield stress (MPa)
S1	60	0.25	300
S2	40	0.25	260
S3	30	0.25	240
S4	10	0.25	240
S5	5	0.25	120
S6	1	0.20	60

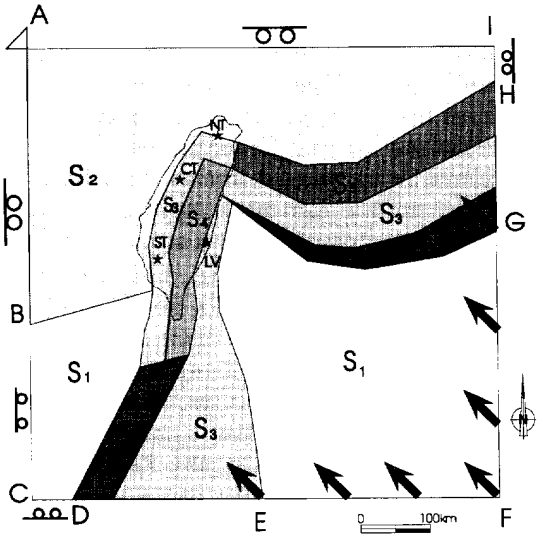

Fig. 5. Geometry and boundary conditions of the finite-element model of Taiwan collision. For geographic coordinates, see Fig. 1a; coast of Taiwan shown as thin dotted line. S_1, S_2, S_3, S_4, S_5, and S_6, subdomains with different rheologies (Young's modulus, Poisson's ratio and yield stress listed in Table 3). Uppercase letters $A-I$ indicate segments of frame with different boundary conditions: open triangle = fixed boundary (point A); open circles = roller in one direction (N–S for AB, E–W for AI); no symbol = free segments (BC, CD, DE, IH and GH); large black arrows = common direction of displacement based on plate kinematics (EF and FG). Location of references site added (see also Fig. 4).

4.2. Significance and limitations of 2-D finite-element analysis

We focus on aspects of the collision zone where continental crust deformation is dominated by brittle

processes, which can be approximated by an elastic and elasto-plastic rheology at the scale considered. The elasto-plastic yield limit obviously varies with depth, so that the values adopted represent an average effective yield strength for the model. The depth considered for the brittle deformation is about 20–30 km. Most surface earthquake hypocentres concentrate in the depth range 0–15 km, that is the upper half of the continental crust (e.g., Chen and Molnar, 1983; Gough and Gough, 1987). Bott (1990) pointed out that the uppermost 20 km of the continental crust is elastic, representing the strong and cool layer of the upper lithosphere. However, in the subduction zones, where cold lithosphere is underthrust, elastic behaviour occurs at greater depths. Ranalli and Murphy (1987) showed that the depth-dependence of lithospheric rheology varies with tectonic provinces; in many cases the continental lithosphere includes one or two soft ductile layers sandwiched between brittle layers. For example, for Mesozoic–Cenozoic continental convergence zones, brittle behaviour may occur either in the upper crust (20–30 km) and in the uppermost mantle (60–80 km). Viallon et al. (1986) have used a thickness of 60 km to represent an average level of the mechanical lithosphere for the elasto-plastic model; the deformation at such depths normally includes viscose deformation, which probably explains why they used $n = 0.49$, a high value of the Poisson ratio, in their elasto-plastic model. In our model, we aim at discussing the brittle deformation in the upper crust through a simplified 2-D analysis.

The 2-D models used for the first-order approximation are of course largely simplified in comparison with actual patterns; they do not allow consideration of various significant stress effects due to topography, buoyancy, basal drag, coupling at depth and thermomechanical deformation within the lithosphere. For instance, the possible presence of a mechanically weak layer at midcrust depths in a continental lithosphere, which could result in mechanical decoupling of the crustal layers, is not considered. Partial decoupling is also present in the convergence zone, where slip occurs oblique to the plate margin, between parallel zones of strike-slip faulting and underthrusting. Both these phenomena (on horizontal and dipping surfaces, respectively) were not considered in our 2-D modelling experiments discussed herein; to elucidate such decoupling problems, we tried to build local 2-D and 3-D models using the distinct element method around the Longitudinal Valley (work in preparation).

We chose to use plane stress conditions ($\sigma_{zz} = 0$), which correspond for a two-dimensional model to an 'infinitely thin' plate, where thinning or thickening is however possible. Under this condition, the vertical component of stress is zero, or is small relative to the horizontal component of stress.

4.3. Configuration of the model

The geometry of the model is represented by a rectangle which covers a rectangular area from 19°N to 27°N, and from 118°E to 127°E (Fig. 5). This size is sufficient to prevent edge effects from disturbing the stress field in the area of major interest (the island of Taiwan) near the centre of the rectangle. The model contains 519 triangular linear elements, with three nodes in the summits, and 996 nodes. The grid has been designed and modified to permit assignment of varying rigidities for different tectonic units, according to multiple constraints and to the probable roles of these units in the tectonic processes (Fig. 5).

The ten sub-units of the model represent major structural units according to the regional tectonic setting. These units are in fact separated either by transition zones (e.g., the passive margin between the continental shelf of Eurasia and the oceanic floor of the South China Sea) or by major faults or discontinuities (e.g., the different units of the Taiwan mountain belt; compare Figs. 1b and 5). Around Taiwan, we defined these boundaries by taking the bathymetric data and the earthquake distribution into account. However, a rigorous introduction of physically constrained parameters for all features is not feasible. In detail, some aspects of the plate boundary geometry are still uncertain, such as the accurate shape of the major tectonic lines southeast of Hualien (eastern Taiwan). In Fig. 5, the pattern of these boundaries should be regarded as a first approximation, which is reasonable considering the range of other uncertainties, especially in terms of rheological properties.

4.4. Rheology

We divided the region studied into ten subdomains, shown in Fig. 5, with six different properties

listed in Table 3. The main criteria to define these major rheological properties deal with geological composition (oceanic crust, continental crust, island arc crust, foreland belt, metamorphic belt, accretionary prism), crustal thickness and thermal state (e.g. the Okinawa Trough area), etc. The materials themselves are considered homogeneous and isotropic. Within the general simplifications of the model, the choice of elastic constants offers a good approximation. The elastic constants include two parameters: Young's modulus and Poisson's ratio. For the elasto-plastic deformation, a third parameter, the yield stress, is added. The actual values of these parameters are of course not well constrained; as a consequence, we tested models with a variety of values in order to explore the effects of changes in parameters and the sensitivity of our results to various choices. These numerous attempts cannot be described herein; it is interesting to mention that patterns of stress trajectories obtained depend little on the values of the elastic constants within a reasonable range of choices. The values finally retained (Table 3) should be regarded somewhat arbitrary, and have been chosen in order to be compatible with a better fit of the model calculated. However, a model with, for instance, the constants made equal throughout the plate boundary zone (i.e., $S_3 = S_4 = S_5$) gave similar results.

For the elasto-plastic model shown in Fig. 6, we have used the elasto-plastic behaviour with the Von Mises criterion. This law takes into account both the elastic deformation of the lithosphere submitted to low stress and the plastic deformation under large continuing stresses. Three parameters describe the material (Table 3): Young's modulus, Poisson's ratio, and the yield stress. Because several major structural units have quite different rheological properties, several subdomains have been distinguished in the case of the Taiwan collision area, corresponding to different tectonic settings (Fig. 5 and Table 3). Young's modulus thus ranges from the highest value in the oceanic lithosphere of the Philippine Sea plate and the South China Sea (S_1 in Fig. 5) to the lowest value in the thinned lithosphere of the Okinawa Trough back-arc basin (S_5 in Fig. 5). Various intermediate values were attributed to continental shelf and margins (S_2 in Fig. 5), island arcs (S_3 in Fig. 5), outer and inner mountain belt (S_3 and S_4, respec-

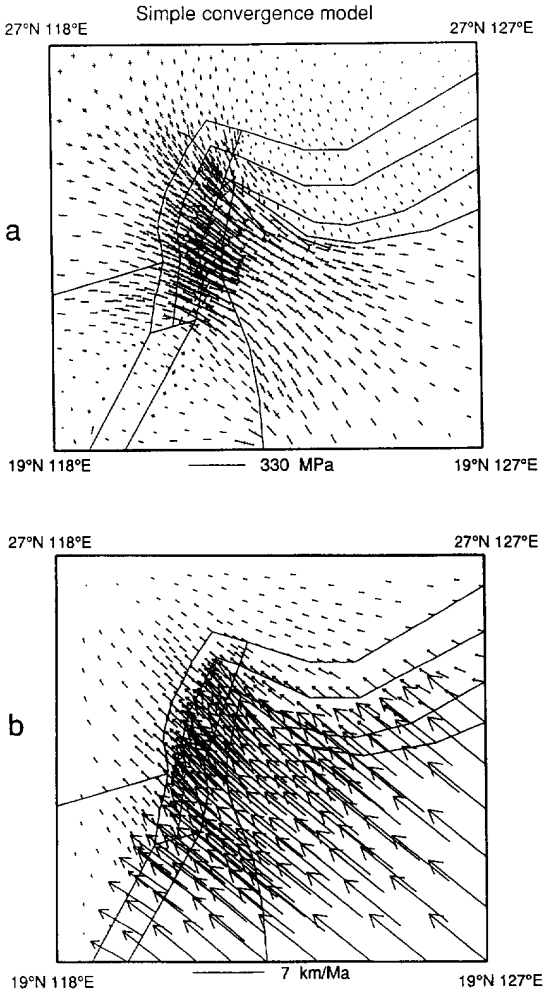

Fig. 6. Stress distribution and horizontal velocity field calculated in the 2-D finite-element elasto-plastic model of simple convergence (structure, rheology and boundary conditions defined in Fig. 5 and Table 3). Thin lines correspond to changes in rheology (see Fig. 5). Scale of stress magnitudes shown before the frame. (a) Principal stresses in the horizontal plane, shown as small couples of arrows. Pairs of convergent arrows represent maximum compressive stress. Note the stress concentration in the Taiwan collision zone, the fan-shaped distribution throughout the island and the pronounced stress trajectory deviation near the northwestern corner of the Philippine Sea plate. Compare this model with the actual stress distribution (present-day and Quaternary) reconstructed from geophysical and geological data (Figs. 3 and 4). (b) Horizontal velocities. The vectors indicate the velocities at the displaced grid points, relative to Eurasia. Velocity scale shown below the frame.

tively, in Fig. 5) and the Okinawa back-arc basin (S_5 in Fig. 5). All these values are indicated in Table 3. Abnormally low values of Young's modulus and yield stress (with also a lower Poisson ratio, that is, a more compressible material) were added along the subduction zones of the Ryukyu Trench and the Manila Trench (S_6 in Fig. 5). These low values (Table 3) reflect the presence of mechanical decoupling and easier convergence at trenches.

The values that we adopted for rheology are certainly not well constrained. Consequently, we used models with a variety of values in order to explore the effects of changes in these parameters and the sensitivity of our results to their choice. We found that the patterns of stress trajectories have very little sensitivity to the absolute values, and that they are moderately influenced by the ratios of these parameters, which indicates that the geometry and boundary conditions play the greatest role in the model.

4.5. Boundary conditions

For the parameters of the boundary conditions, we have used velocities (or displacements) instead of forces (or stresses), because the latter are difficult to estimate, whereas the velocity of plate movement between the Philippine Sea plate and the Eurasian plate is well known (Table 1). The northwestern corner of the model is fixed (point A in Fig. 5); under this condition, displacement is left free along the E–W direction for the northern boundary (AI in Fig. 5) and along the N–S direction for the northwestern boundary (AB in Fig. 5). The results showed that deformation occurring along these segments, AI and AB, is in fact negligible with respect to those occurring near the plate boundary, in agreement with geological observation. For the southeastern boundaries of the model (EF and FG in Fig. 5), we imposed a constant displacement in the direction of plate motion, according to the kinematic parameters of Table 1. Note that we also tried to apply different displacements as functions of latitudes and longitudes along the boundaries EF and FG, based on the calculation of the angular velocity between the Philippine Sea plate and Eurasia (Table 1): this more sophisticated application led to similar results, demonstrating that applying a constant displacement vector at these boundaries is enough (Fig. 5).

Concerning the segments BC, CD, DE, IH and GH of Fig. 5, we have left them free (segments CD–DE and HG correspond to transverse sections of the deformed plate boundaries). We have also tried to set the BC, CD and IH segments with motion allowed in the sole N–S direction (BC and IH) or the sole E–W direction (CD): the resulting distributions of stress trajectories were similar and these changes had no influence in the central region of the model. In some numerical models, introducing different boundary conditions result in dramatic change in stress distribution (e.g., Vilotte et al., 1982), which also depend on basic choices such as for plane stress or plane strain condition. Although they are not described herein, numerous experiments were consequently made, with different combinations of reasonable boundary conditions along segments AI and AB, BC–CD and HI ('stable' Eurasia), as well as DE and HG (deformed plate boundary zones). Differences remained small, confirming that such choices are not critical for the model.

We applied initial horizontal displacements in the different possible directions of the plate motion of the Philippine Sea plate relative to Eurasia, based on the plate kinematics parameters shown in Table 1. The imposed displacement in the models of Fig. 6 is 7 cm/yr along the azimuth 310° (i.e., N50°W), based on the latest Seno model (Table 1), for about 1% deformation for the elasto-plastic model (the imposed displacement of 7 km corresponds to a duration of about 1 Ma). The imposed displacement in the elastic model was 0.07 km (i.e., a duration of about ten thousand years).

As expected for an elastic model that fails to take into account the stress-buffering effects of yielding, purely elastic models (not illustrated herein) produced stresses that were progressively larger, and unrealistic, with increasing amounts of displacements. In the elasto-plastic model, the magnitudes of stress decrease more rapidly away from the collision zone than in the elastic model and the stress concentration in the Philippine Sea plate east of Taiwan decreases. We thus consider that the elasto-plastic model provides more realistic results, taking into account the actual distribution of compressional deformation indicated by the seismotectonic studies mentioned earlier, and also the geodetic data from the first GPS network surveys (Yu and Kuo, 1994).

Most of the deformation effectively concentrated in Taiwan. We consequently decided to describe the elasto-plastic model (Fig. 6) rather than the elastic one.

5. Simple convergence model of Taiwan

5.1. General distribution of calculated stresses

We determined the stress (Fig. 6a) and displacements fields (Fig. 6b) throughout the grid as caused by the boundary conditions (Fig. 5). With all the characteristics and constraints discussed above, we obtained by our numerical modelling the calculated stress pattern illustrated in Fig. 6a for the simple convergence model (to be compared with the observed stress patterns reconstructed in Figs. 3 and 4, especially in terms of σ_1 trends). The boundary displacement simply corresponds to the convergence of the Philippine Sea plate relative to Eurasia (Fig. 5 and Table 1). The calculated stress trajectories exhibit a dominant NW–SE compressional stress pattern in the Taiwan area and a typical fan-shaped distribution, with a spread angle of about 50°. Despite local discrepancies, which will be discussed later, these computed stress orientations are similar to the palaeostress trends reconstructed from field data, as a comparison between Figs. 4 and 6a shows. The comparison is made easier in Fig. 7, considering the observed and calculated azimuths of σ_1 axes in the four reference points defined in Table 2 and Fig. 4b. These comparisons are summarized in Table 4, where the local angular misfits are also listed. The average misfit is generally acceptable (about 10 degrees). The largest misfits are smaller than 25 degrees. The smallest misfits (7 degrees) are obtained in eastern Taiwan (point LV, see Fig. 7 and Table 4).

It is important to observe the effect of the weak zone added along the Ryukyu and Manila Trench systems (S_6 in Fig. 5 and Table 3). This effect is somewhat artificial as mentioned before, but it is a reasonable technique for simulating the strong mechanical decoupling along the active subduction zones in 2-D finite-element modelling. Note in Fig. 6a that the stress transmitted largely varies across the decoupling zone; in the case of the Ryukyu Trench, the trends of stress trajectories change also abruptly across the boundary, due to this decoupling.

Taking into account both the simplifying assumptions of the numerical modelling and the angular uncertainties of field determinations, the fit between the calculated stress pattern of the finite-element model (Fig. 6) and that determined based on the geometrical synthesis of field analyses (Figs. 3 and 4) is rather good in general (Fig. 7), so that our model is valid as a first approximation. However, in more detail, the misfit of the calculated palaeostress trends is noticeable and systematically positive (clockwise) in comparison with the reconstructed stress trajectories map (Fig. 7 and Table 4). This discrepancy will be discussed in a later section.

Table 4
Results of maximum stress trends in the four reference sites of Fig. 4b and Table 2, for different experiments based on convergence, a single direction of 310° and few variable conditions

Model	Site	Azimuth of σ_1	Misfit
Simple convergence			
Elasto-plastic model	NT	164	+6
	CT	143	+21
	LV	135	+7
	ST	117	+10
Convergence + trench retreat			
Model 1 (V_c = 15 km/Ma)	NT	16	+37
	CT	154	+32
	LV	126	+4
	ST	116	+11
Model 2 (V_c = 30 km/Ma)	NT	67	+88
	CT	154	+32
	LV	126	+4
	ST	114	+9

The misfit is given relative to actual σ_1 trends indicated in Table 2 (see Figs. 6–9, 11, 12 and 13a). An asterisk is added where the misfit is not significant, due to instability of stress depending on poorly constrained local changes (variation in southward trench retreat near the Taiwan coast).

5.2. Directions of compressional stress and plate convergence

Let us consider the dispersion of compressional stress trends with respect to the direction of plate convergence which induces them in the collision zone. This problem is important because for earlier

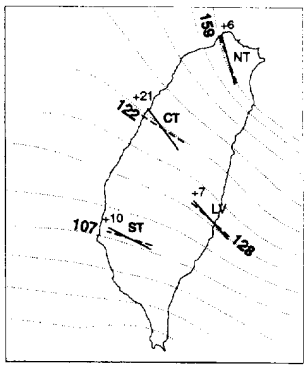

Fig. 7. Results of maximum stress trends and angular misfits at the four reference sites of the simple convergence model. Azimuths and misfits in degrees. Misfit given relative to observed σ_1 trends (+ = clockwise; − = counter-clockwise). Observed stress trajectories as dotted lines (from Fig. 4).

steps of the collision process the orientation of compressional stress used as a key to reconstruct the direction of plate convergence (Angelier et al., 1986).

Adopting as a reference the direction of motion of the Philippine Sea plate relative to Eurasia, a 10° counterclockwise deviation of maximum compressional stress occurs in southern Taiwan (Fig. 4b). A similar deviation is observed in the model of Figs. 6 and 7 (azimuths 117°–164°, the actual ones being 107°–159° in Fig. 4). With the same reference direction, in northern Taiwan, the deviation of stress trajectories reaches 37° clockwise, and occurs within a short distance. The geographic changes in compressional stress trends are thus pronounced in northern Taiwan, north of 24.5°N and east of 121°E (azimuths 107°–159° in the data of Fig. 4, 117°–164° in the model of Figs. 6 and 7). In both cases, these deviations in the model are consistent with the results of field observations. We infer that the asymmetric distribution of stress trajectories around the north of Taiwan is caused by the geometry of the plate boundary (especially, the presence of the sharp northwestern corner of the Philippine Sea plate) and by the oblique collision of the Philippine Sea plate;

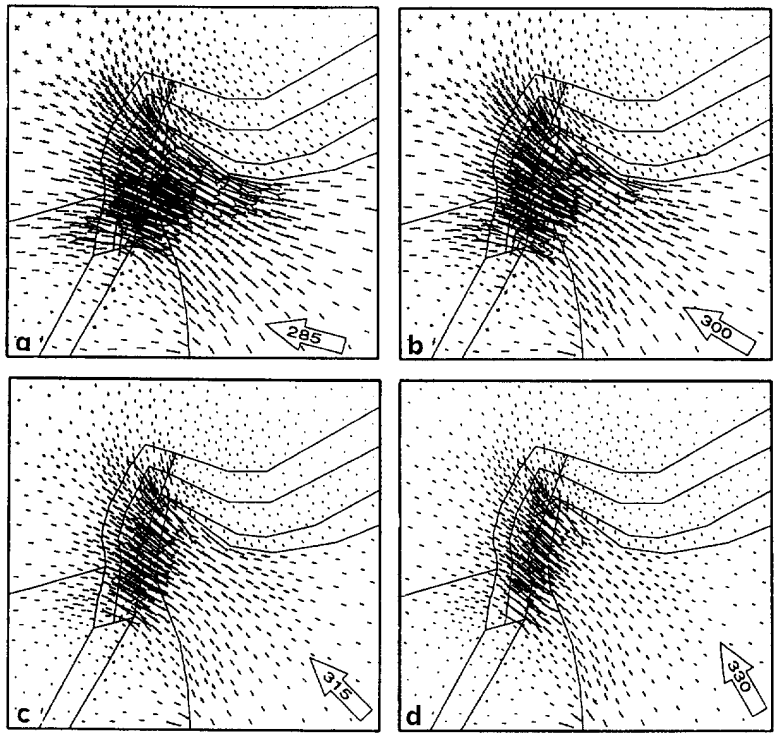

Fig. 8. Influence of the direction of the motion of the Philippine Sea plate relative to Eurasia with the elasto-plastic model. Azimuths of convergence: (a) 285°, (b) 300°, (c) 315° and (d) 330°. Same symbols as in Fig. 6. See also Table 5.

in other words, this distribution is strongly influenced by the shape of the collision indenter.

5.3. Effect of variation in the direction of convergence

One purpose of our study is to determine how far the direction of convergence applied to the boundaries of the model influences the stress trajectories. We have studied the effect of changes in the direction of plate motion, with azimuths of motion varying from 285° (N75°W) to 330° (N30°W) in four steps; the results are shown in Figs. 8 and 9 and Table 5. These results can be compared with those obtained from the actual azimuth of convergence, 310° (Figs. 6 and 7), and also with the actual compressional trends obtained from seismotectonic data (Figs. 3 and 4). A surprising feature is the better fit with an azimuth 285° of convergence, although the counterclockwise deviation of this azimuth relative to that of actual convergence (310°) is unacceptably large (25°, see Table 1).

There are certainly appreciable changes in the general trends of stress trajectories in our models as a function of the direction of convergence (Figs. 8 and 9 and Table 5). However, this deviation of stress trajectories remains smaller than for the previous model by Huchon et al. (1986), in which a rotation of 40° in the direction of convergence resulted in a deviation of about 20° of the whole stress field. In our simple convergence models, the rotations of stress field induced by a rotation of 45° in the motion of the Philippine Sea plate relative to Eurasia (Fig. 8) average 8° in northern Taiwan, 13° in central Taiwan, 9° in the Longitudinal Valley, and 16° in southern Taiwan. In detail, these changes are illustrated at the four control points in Table 5 and Fig. 9

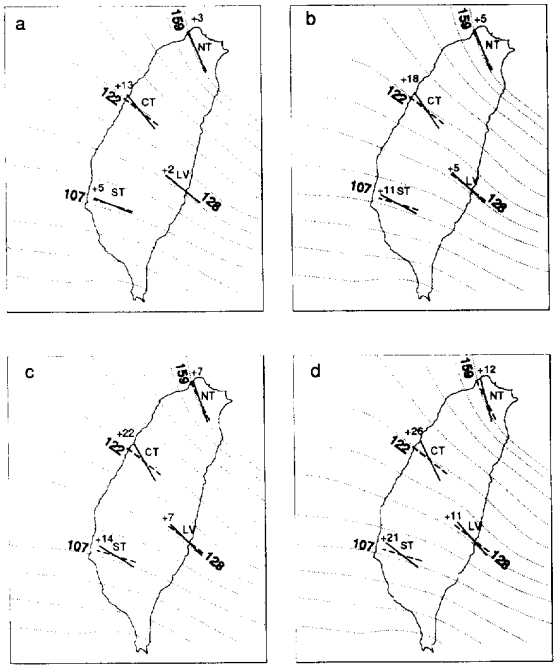

Fig. 9. Comparison of angular misfits obtained with the models of Fig. 8. Same symbols as in Fig. 7. See also Table 5.

(showing the observed and calculated trends of compression). Thus, a variation as large as 45° in the direction of plate convergence (azimuths 285° and 330°, see Table 5) results in a variation as small as 9°–16° in the trends of maximum compressional trends for the whole Taiwan area.

Lee (1986) pointed out that a rotation of 30° in the direction of plate convergence cannot result in the pronounced deviation of the stress; he explained this effect in terms of the presence of the weak decoupling zone, the Longitudinal Valley Fault. Although we did not involve in our models the effect

Table 5
Results of maximum stress trends for different convergent directions between the Philippine Sea plate and Eurasia

Site	Azimuth of σ_1 for convergence 285	Azimuth of σ_1 for convergence 300	Azimuth of σ_1 for convergence 315	Azimuth of σ_1 for convergence 330
NT	162 (+5)	164 (+5)	166 (+8)	171 (+12)
CT	135 (+13)	140 (+18)	144 (+22)	148 (+26)
LV	130 (+2)	133 (+5)	139 (+11)	139 (+11)
ST	112 (+5)	118 (+11)	121 (+14)	128 (+21)

The numbers between parentheses refer to the difference between the results of modelling (Figs. 8 and 9) and geological data (Fig. 4).

of weakness or decoupling along the Longitudinal Valley, we observe such a limited rotation of the stress field for large rotation of the direction of convergence. This suggests that this relative stability of the stress pattern regardless of the direction of convergence is principally dependent on the whole configuration of the plate boundaries. We infer that the average trends and the deviation of stress trajectories are controlled by the direction of convergence in a limited way (Fig. 8), and that they are much more influenced by the geometry of the plate boundary, the presence of the sharp northeastern corner of the Philippine Sea plate playing a major role (Figs. 1 and 4b and Fig. 5).

To conclude, we obtained in our simple collision models a major compressional stress pattern with a NW–SE direction in the Taiwan area and a NW–SE trend in the Ryukyu Arc area (Figs. 6 and 7). The fan-shaped pattern of stress trajectories is principally controlled by the angular shape of the collision zone, so that the dependence of stress trends on the direction of convergence is attenuated: an angular change of 45° in this direction results in a much smaller variation of stress trends, of about one third in the same sense.

6. Convergence–trench retreat model

6.1. Limits of simple collision models: northeastern Taiwan

Northeast of Taiwan, the Okinawa Trough area is dominated by extensional tectonics (Kimura, 1985; Letouzey and Kimura, 1985, 1986; Sibuet et al., 1987), and the extensional regime is present in northeastern Taiwan, especially near the Ilan Plain as discussed in a previous section (Tsai, 1986; Yeh et al., 1989, 1991). It is tempting to account for this extension through a model of lateral extrusion related to the Taiwan collision. At a different scale and for different periods, following a suggestion by Tapponnier et al. (1982), Peltzer (1988) proposed that the indentation of a block plasticine free to move on one side and indented by a rigid body results in the lateral extrusion of blocks and formation of vacuums in between: they used this model to explain the opening of the Andaman Sea and the South China Sea basin, as a result of the India–Eurasia collision. Numerical modelling was also used for discussing the results of the continental collision between India and Asia (Vilotte et al., 1982; England and Houseman, 1989).

We first designed different models, not discussed herein, in order to reproduce the extensional field of the western Okinawa Trough area as a simple consequence of the Taiwan collision. These attempts at producing extension as the result of lateral extrusion which accompanies the indentation of the Eurasian margin by the Philippine Sea plate in Taiwan were unsuccessful. Effectively, the 2-D simple convergence models of the Taiwan region discussed in the previous section fail to produce enough extension in the Okinawa Trough and northeastern Taiwan area (Fig. 6). We infer that the suction force related to the southward retreat of the Ryukyu subduction zone, which was not involved in these models, plays a major role in this extension.

6.2. Estimate of southward trench retreat rate

We consequently tried to evaluate the opening of the Okinawa Trough, which probably influences the stress field in the northeastern Taiwan area. As the actual distribution of the forces is difficult to estimate on the northern side of the Ryukyu Trench, including the Ryukyu Arc and the Okinawa back-arc basin, we have modified the boundary conditions as little as possible, and examined what should be added in the model with simple collision and subduction in order to explain the observed stress patterns. The present geodynamic and kinematic knowledge of this region does not allow development of a more detailed model, because the results would not be controlled by data significantly. We thus obtained a model involving additional southward displacement of the front of the Ryukyu Arc. This displacement is in fact related to combined trench retreat in the Ryukyu Arc and back-arc spreading in the Okinawa Trough area.

It is possible to implement the roll back effect by applying forces at the trench (Wortel and Cloetingh, 1985; Viallon et al., 1986). However, determining the balances of forces near the trench area (ridge push, slap pull, drag force, compositional buoyancy, plate contact resistance, etc.) involves complicated

calculations and assumptions (England and Wortel, 1980; Wortel and Cloetingh, 1985; Bott, 1991; England and Molnar, 1991; Wortel et al., 1991), and depends on several parameters, which are poorly constrained in the case of the trench segment considered herein. As a consequence, we used displacement data because they are better controlled than stress magnitude data. We thus used the nodal velocity instead of the forces. Note, however, that we also carried out some experiments with forces applied at the trench (not described herein), and we obtained similar results.

For the simulation of this displacement, a velocity must be determined, which requires consideration of the spreading rate of this region. Letouzey and Kimura (1985) suggest a spreading rate of about 46 km/Ma for the southern Okinawa Trough, based on the study of magnetic anomalies. It is reasonable to consider that the retreating rate of the Ryukyu Trench is smaller than the opening rate of the Okinawa basin, due to shortening in the Ryukyu accretionary prism between the Ryukyu Arc and the Ryukyu Trench. We consequently adopted a retreating rate of about 15 km/Ma for the model of Fig. 10a. We applied this velocity at the Ryukyu Trench boundary as an internal initial nodal displacement for simulating both the opening of the Okinawa and the retreating of the Ryukyu Trench. There is no other difference between this model and the previous one (compare Figs. 5 and 10a).

We set the retreating rate to zero near Taiwan (because the Okinawa Trough extension obviously disappears west of the Ilan Plain), with a linear increase from west to east between 122°E and 123°E (Fig. 10a). In order to evaluate the influence of this additional southward displacement of the Ryukyu Trench, we carried out experiments with various velocities. The results obtained with a rate of 15 km/Ma are shown in Figs. 10b and 11 ('model 1'; Table 4); the results with a higher rate of 30 km/Ma along the Ryukyu Trench front and 15 km/Ma near Taiwan are summarized in Fig. 11 ('model 2', Table 4). These values are somewhat arbitrary, and have been chosen in order to produce the distribution of extension observed in reality. Fig. 12 and Table 4 allow accurate comparison between these two models, in terms of stress trend misfits at the four control points already discussed.

6.3. Effect of Ryukyu Trench retreating

The results of this new modelling defined in Fig. 10a are shown in Figs. 10b, 11–13a. These maps illustrate a dramatic change relative to models of Figs. 6–8: extensional stress, which could not be obtained in these previous models, now dominates in the Okinawa Trough–Ryukyu Arc region. Furthermore, this extension is oriented N–S (Figs. 10b and 13b), which is consistent with seismotectonic data

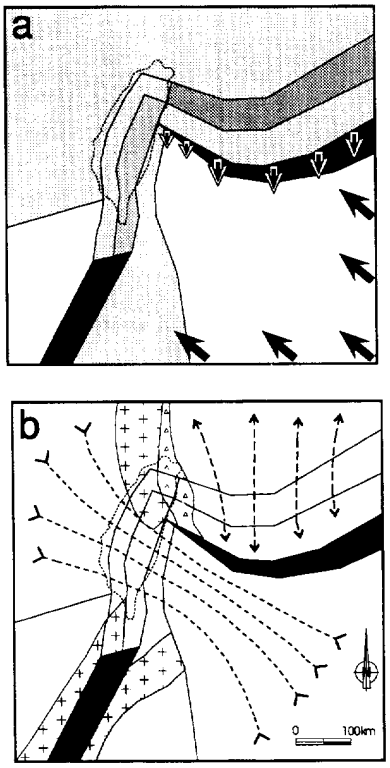

Fig. 10. (a) Geometry and boundary conditions of the finite-element model with collision and trench retreating. Same explanations as for Fig. 5, the only difference being the addition of a southward displacement at the Ryukyu Trench axis (southward-directed arrows). Rheological parameters and boundary conditions given in Fig. 5 and Table 3. (b) Resulting tectonic regimes and the trajectories of σ_1, based on the convergence–trench retreat model 1 (see Table 4). Dashed lines with convergent arrowheads indicate compressional trajectories in the area of pure compression. Dashed lines with divergent arrowheads indicate extensional trajectories in the area of pure extension. Open triangle pattern indicates regions of transtension; pattern of crosses indicates regions of transpression. Zone of decoupling in dark grey.

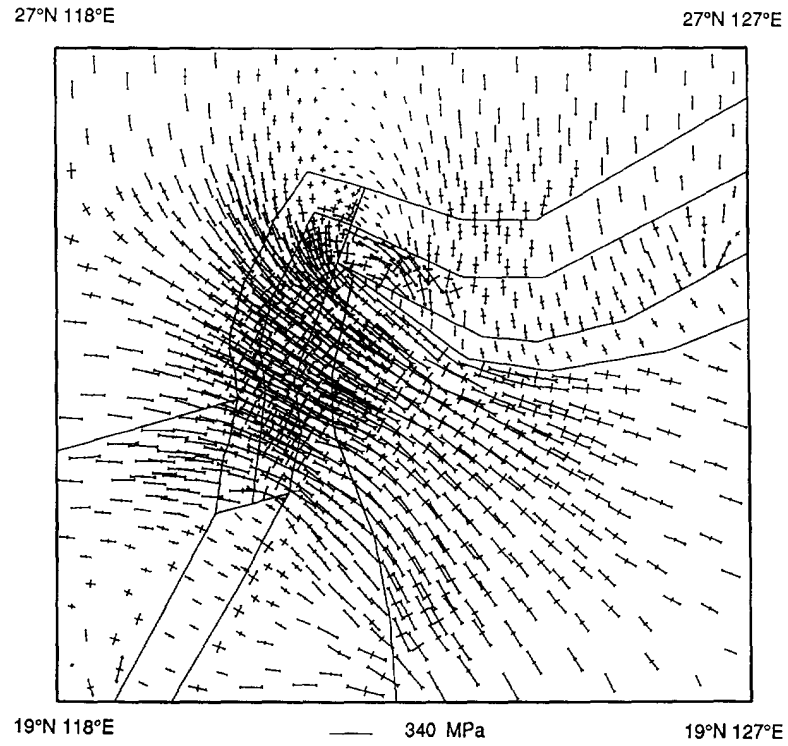

Fig. 11. Stress distribution calculated in the convergence–trench retreat elasto-plastic model (model 1 in Table 4). Structure, rheology and boundary conditions defined in Fig. 10a and Table 3. Same symbols as in Fig. 6. Pairs of divergent arrows represent minimum extensional stress, especially northeast of Taiwan, in the Okinawa Trough area, where N–S extension occurs contrary to Figs. 6 and 8.

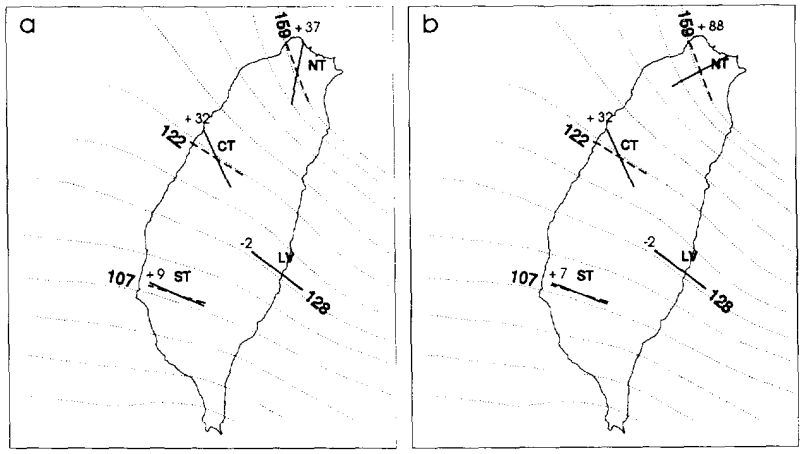

Fig. 12. Results of maximum stress trends and the misfits of the convergence trench-retreat models 1 and 2: (a) model 1, (b) model 2. Same explanation as for Fig. 7. Note that significant variation in trends occurs in northeastern Taiwan exclusively.

available in the western Ryukyu Arc and the Ilan Plain (Yeh et al., 1991).

As a consequence, our model predicts that in northeastern Taiwan, some transitional zones may develop between the pure compressional tectonic regime (which characterizes most of the collision zone of Taiwan) and the extensional tectonic regime (which dominates in the northeastern portion of the model). The transition in the stress field is characterized by two intermediate regimes where significant occurrences of strike-slip deformation mode can be expected: one is mostly compressional, the other one is mostly extensional. In Figs. 10b and 13b, these intermediate regimes, marked with patterns of crosses and triangles (respectively), are located in northern Taiwan, between the main collision belt and the western tip of the Okinawa Trough. Southwest of these areas, in the central collision belt of Taiwan, NW–SE compression occurs; to the east, in the Ryukyu Arc–Okinawa Trough system, N–S extension dominates (Figs. 10b and 13b). Moving from west to east across these transition zones, the relative magnitudes of stress vary from compression to extension, so that the whole stress regime changes to extension.

The velocity of the southward displacement of the Ryukyu Trench boundary plays a significant role in these improved models, as illustrated by the comparison between two examples (referred as models 1 and 2 in the lower half of Table 4). The sole difference between these two models lies in the velocity of the maximum displacement, 15 km/Ma in the first (Figs. 10 and 11) and 30 km/Ma (Fig. 13). Comparing the main stress regimes summarized in Figs. 10b and 13b, or the detailed stress distribution shown in Figs. 11 and 13a, one observes that the extensional area rapidly moves from east to west as this velocity increases (considering the distribution of stress regimes in Figs. 10b and 13b), it is clear that the pure extensional regime of the Okinawa–Ryukyu system limits offshore Taiwan with the 15 km/Ma model. In this respect, the second model is less realistic than the first one, which suggests that under the simplifying assumption of the general modelling process a limited southward velocity is reasonable (Figs. 10 and 11) amounting to one third of the spreading rates suggested by Letouzey and Kimura (1986) for the southern Okinawa Trough.

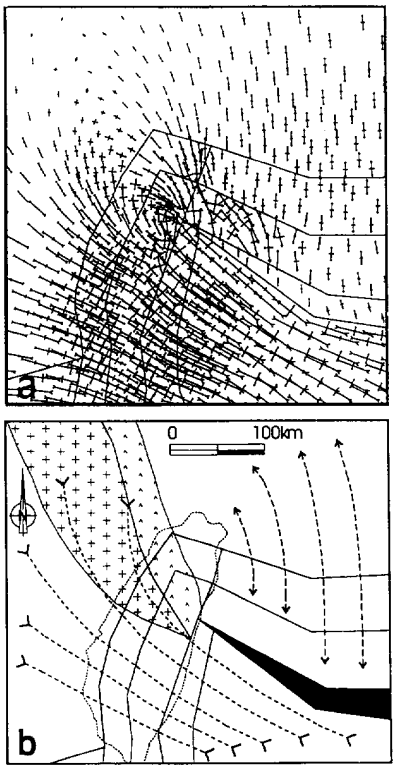

Fig. 13. Influence of southward trench retreat velocity. (a) Stress distribution calculated in the convergence–trench retreat elasto-plastic model (model 2 in Table 4). Entire model area not shown (compare with Fig. 6a). Same explanation as for Figs. 10 and 11, the only difference being an increase of velocity of trench retreat southward (see text). Note the westward shift of the transition zone relative to Fig. 10. Note also the local occurrence of the ENE–WSW extensional stress trends in northeastern Taiwan. (b) Schematic stress patterns, σ_1 trajectories and σ_3 trajectories correspond to the model partly shown in Fig. 11a. Same explanation as for Fig. 10b. Note that the main difference, relative to Fig. 10b, is a westward shift of the transition from compression (Taiwan) to extension (Ryukyu).

However, neither the major trends of extension (roughly N–S across the Okinawa–Ryukyu system) nor those of compression (NW–SE in the centre of Taiwan) are significantly affected by such changes of southward displacements. Fig. 12 shows that there is no difference, except in northern Taiwan.

6.4. Comparison with simple convergence models

A simple comparison between the two simple convergence models and two convergence–retreating

models can be made at the four reference sites defined in Table 2 and Fig. 4b. The corresponding results are listed in Table 4, including the local angular misfits.

First, such a comparison illustrates the extent of changes in stress regime and trajectories in the northern half of Taiwan as related to the behaviour of the Ryukyu Trench boundary (left free in the first two models, with imposed southward displacement in the last two ones). Focusing on the models which include trench retreat, the first one shows the NNE–SSW σ_1 trends in northern Taiwan (site NT), whereas the second ones (with increased velocity) shows ENE–WSW σ_1 trends (Table 4 and Figs. 10, 11 and 13). This difference illustrates the high sensitivity of the stress regime in northern Taiwan to variation of boundary conditions in the Ryukyu Arc–Okinawa Trench area.

Second, despite this strong influence of trench retreat velocity on the predicted stress patterns in northeastern Taiwan, it is important to observe that at a short distance further south, these effects are diminishing and practically vanish in the southern half of Taiwan. The variation in retreat velocity does not affect the azimuth of σ_1 in central Taiwan (although this trend, 154°, still differs markedly from those of the simple convergence models, 143°: see Table 4). Further south, in southern and eastern Taiwan, the directions of σ_1 remain practically unaffected: these azimuths average 120° (126° and 114° in sites LV and ST, respectively, see Table 4), that is, almost the same values as for the simple convergence models (135° and 117° on average in the same sites: Table 4). We conclude that the effects of the suction force related to the Ryukyu subduction zone play a very important role locally, in northern Taiwan, but have very little influence further south in most of the collision zone.

7. Discussion

7.1. Misfit of stress distribution

The models presented herein and used to calculate the stress distribution have been drastically simplified with respect to the actual structure and tectonism near Taiwan. However, they provide a rigorous framework (Figs. 5 and 10a; Table 3) for interpreting the stress distribution observed (Figs. 3 and 4; Table 2), in relation to the major features and kinematics of this collision–subduction area (Figs. 1a and 2a; Table 1). In terms of angular misfits between observed and computed trends of maximum compressional stress, the general agreement is rather satisfactory (compare Figs. 4, 6 and 7; Table 4). In this respect, our models provide the same general consistency as for previous ones (Huchon et al., 1986; Lee, 1986; Viallon et al., 1986). A major difference is the better control of the actual stress distribution in our model (Figs. 3 and 4), because many geological and geophysical analyses published during the last eight years constrain it better.

In more detail, the misfits between observed and calculated trends of compression range between 6 and 21 degrees (Table 4 and Fig. 7), the larger local variation being not considered in northeastern Taiwan. Such misfits (shown with asterisks in Table 4) are not really significant, because they result from a combination of poorly constrained effects of the shape of the northwestern corner of the Philippine Sea plate (Figs. 2a and 5) and variable influence of the neighbouring Okinawa–Ryukyu extension (Table 4; Figs. 10, 11 and 13). To the south, both these effects vanish across a more regular collision boundary trending NNE–SSW over a distance of about 200 km (Fig. 1b). Figs. 7, 9 and 12 allow fast comparison of these misfits at four characteristic locations in Taiwan.

Furthermore, the misfit of the calculated palaeostress trends is systematically positive (i.e., clockwise) in comparison with the reconstructed stress trajectories stress map (Table 5). As a result, the smallest average misfit is obtained in a model with an azimuth of 285° of Philippine Sea–Eurasia convergence (Table 5), although the azimuth of 310° is certainly more realistic (Table 1). The difference, however, remains minor (few degrees, compare Tables 4 and 5).

As the first explication of this small but noticeable discrepancy, we observe that the presence and shape of a sharp northwestern corner of the Philippine Sea plate in the model (Fig. 5) strongly influences the clockwise stress deviation in northern Taiwan. This effect is maintained if the direction of convergence of the Philippine Sea plate is modified

(Fig. 8). Unfortunately, the actual submarine structure and distribution of deformation off Hualien (Fig. 1b) are still poorly controlled by geophysical and geological data, so that the actual shape of the major tectonic boundary remains unknown in detail. Because the misfit variation as a function of convergence azimuth remains approximately constant regardless of the location in Taiwan (the misfit increases about 10° when the convergence azimuth changes from 285° to 330°, see Fig. 8), this first local effect is probably minor.

Secondly, our model ignores by definition the effects of possible decoupling across the narrow Longitudinal Valley Fault zone. This effect, which cannot be estimated rigorously, allows a counterclockwise variation of the maximum stress trends due to the existing shear component; that is, the angles between the maximum compressional stress axes and the trend of the major fault are larger than expected in our models. Such effects are well known across the active strike-slip fault. The plate boundary reflects a zone of weakness, which, given a high normal stress component transmitted from the regional stress field, can only sustain a lower shear stress. Subsequently, stresses rotate to a direction perpendicular to the zone of weakness (Mandl, 1988), and consequently stress patterns are closely related to the geometry of the boundary. For instance, Mount and Suppe (1992) showed that the maximum horizontal stress trends make high angles (70°–90°) with the trends of the active San Andreas Fault in California and the Great Sumatran Fault in Sumatra, because such large crustal-scale strike-slip faults may be inherently weak surfaces. Faulting and crustal deformation along such weak tectonic boundaries may be controlled by 'strong crust and weak transformation'. The shear stress in the crust appears to be generally high (i.e., consistent with Byerlee's law), whereas the shear stresses resolved on planes parallel to the transform faults are low. However, the cases discussed here are quite different, because the major boundary, the Longitudinal Valley Fault zone, is not a pure strike-slip fault but a thrust with a minor left-lateral component. The dip angle of the active Longitudinal Valley Fault is about 55° (Tsai et al., 1977) and a large thrust component is present (Hsu, 1962, 1976; Tsai et al., 1977; Barrier, 1986) and could be estimated accurately (Yu and Liu, 1989; Lee and Angelier, 1993). As a result, the mechanical coupling is probably higher than in the cases mentioned above. However, some results of tectonic analyses of Quaternary faulting suggest that a local counterclockwise deviation of compressional stress may occur across the Longitudinal Valley, so that limited mechanical decoupling may occur and contribute to the regional counterclockwise deviation of stress west of the Longitudinal Valley. As a result, some clockwise deviation of stress is suspected in our model (Table 4) relative to the trends expected while taking decoupling into account, because we did not consider the occurrence of such phenomena in the collision zone.

The quality and the quantity of the selected field data also limit the validity of comparisons between calculated and observed stress, especially in northern Taiwan where these data are scarce (Fig. 4). Based on Lue et al. (1991) and Lee et al. (1991), the geomagnetic data showed that a clockwise rotation of about 0–25° is common in northern Taiwan. The models used here do not involve discussion of the rotation of the local small blocks, which are due to the cumulative effects of the oblique convergence of the Philippine Sea plate. These effects have little influence in our models, because we only consider the most recent step in the evolution of the collision zone and the stress orientation data that are used (Fig. 4) correspond either to the Present (Figs. 3a and 3b) or to a relatively short time span (Fig. 3c). Considering all the aspects discussed above and the drastic simplification of the models, the average misfit of about 5–15° in northern Taiwan (Table 4) is acceptable.

7.2. *Extension in the Okinawa Trough*

The models taking only the convergence of the Philippine Sea plate into account failed to produce the extensional tectonic regime observed in northeastern Taiwan and the Okinawa basin–Ryukyu Arc area (Fig. 3d). As a result, the role of the opening of the Okinawa Trough and the retreating of the Ryukyu Trench must be acknowledged and incorporated in the models (Figs. 10, 11 and 13; Table 4). Letouzey and Kimura (1985) argued that mechanisms such as trench retreat could maintain extension but do not produce it. Viallon et al. (1986) suggested that the

collision in Taiwan simply act as an 'anchor point' for the Philippine Sea plate, which together with the retreat of the Ryukyu Trench results in the present accurate shape of the Ryukyu Arc. Whatever the balance of forces, our models confirm that extension in the Ryukyu Arc and the Okinawa Trough cannot be explained by only lateral extrusion as a simple consequence of Taiwan collision.

In our convergence–trench retreat models, the complexity of the computed stress patterns in northeastern Taiwan (Figs. 10b and 13b) reflect the actual present-day stress field in this area quite well (Fig. 3d). According to the earthquakes focal mechanism data (Yeh et al., 1991) some extensional regimes with NW–SE, NE–SW and N–S nearly horizontal minimum principal stress axes exist in northern Taiwan. Yeh et al. (1991) suggested that only the N–S trends (group '2C') are probably related to back-arc tectonic activity, the NW–SE trends (group '2A') being possibly associated with the volcanogenic process and the NE–SW ones (group '2B') corresponding probably to a permutation of the principal axes. Note that in our models, it was possible to produce these NW–SE and NE–SW trends due to the effect of the opening of the Okinawa Trough and the retreat of the Ryukyu Trench. For a better investigation of the stress field, it is necessary to collect further data, especially concerning extensional tectonics in northern Taiwan.

The westward migration of the Okinawa Trough seems to be the reason for increasing intensity of extension with time in northern Taiwan. The eruption of Quaternary andesitic volcanic rocks is probably the product of the change of stress field in this area, from pure compression to extension. This can explain the clockwise rotation of stress axes from NW–SE to nearly N–S compression, then progressively to E–W extension and finally to N–S extension (Figs. 11 and 13a). As a consequence of this relative instability of stress field, the misfit values shown with asterisks in Table 4 are of little significance, as discussed before. Teng et al. (1992) pointed out that the age variation of the cessation of arc magmatism in northern Taiwan (more recent to the west) is consistent with westward propagation of the Okinawa Trough. It is worthy to note the spatial distribution of five islets spanning approximately 100 km in the offshore area northeast of Taiwan along a N–S to NNE–SSW trend. They belong to the Ryukyu Arc volcanics and their spatial distribution is quite well consistent with the narrow N–S-trending transition zone shown in our convergence–trench retreat model transtension (see Fig. 10b). We infer that these transitions in stress regime (with transpressional and transtensional regimes) related to the location of extension, may contribute to the onset of the magmatism.

7.3. Successive collision steps

Although the main goal of this paper is a finite-element modelling based on the present and recent kinematics and stress in the Taiwan area, we also aimed at understanding the relationships between the earlier kinematics of plate convergence and palaeostress distributions. Based on brittle tectonic analyses, Angelier et al. (1990) divided the palaeostress distribution in the Hsüehshan Range in northern Taiwan into five events; for all the Taiwan island, Chu (1990) identified six events. However, it is doubtful that the kinematic history of the plate convergence has changed dramatically since the beginning of the Taiwan orogen. Lee et al. (1991), based on study of the magnetic fabric analysis, pointed out that two principal lineations were observed in the eastern Coastal Range. This observation is consistent with the earlier identification of two major compressional events during the Plio–Quaternary collision (Angelier et al., 1986). According to these studies, the older event was characterized with NNW–SSE to NW–SE regional trends of compression (Table 6) and the corresponding azimuth of convergence was approximately 335° (Fig. 14a). For the younger event, compressional trends became NW–SE to W–E (Table 6), for an azimuth of 300° of convergence (Fig. 14b).

Our modelling (Fig. 8) indicates of course that the changes in the direction of motion of the Philippine Sea plate relative to Eurasia result in changes in the average trends of the fan-shaped patterns of maximum compressional stress trends, and the results were quite interesting in terms of relationship between amplitudes of rotations. According to our results, the rotation of stress field induced by a counterclockwise rotation of 45° of the direction of plate convergence averages 10–15° counterclock-

Table 6
Trends of stress trajectories at control points of Fig. 4b, based on an earlier model by Angelier et al. (1986)

	Site	Azimuth of σ_1
Recent collision	NT	145 (+14)
	CT	115 (+7)
	LV	105 (+23)
	ST	102 (+5)
Earlier collision	NT	165
	CT	152
	LV	145
	ST	138

Compare with Tables 2, 4 and 5. For the recent collision, the differences with the better constrained trends of Fig. 4 are indicated between parentheses. For the earlier collision: work in preparation.

wise, which is surprisingly little (Fig. 8 and Table 5). As discussed in an earlier section, we suggest that this relative stability of the stress field, with less influence of the direction of convergence than expected, is principally related to the particular configuration of the plate boundary. The situation of stress distribution that prevailed during the last step of the collision (this paper) differs from the previous ones not only because the direction of motion has changed, but also because the configuration of the plate boundary itself has changed (Angelier, 1990). As a consequence, our models are not directly applicable to the earlier steps of the Taiwan collision (work in preparation).

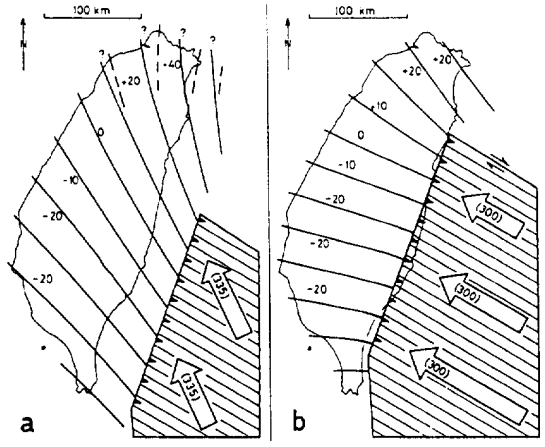

Fig. 14. Stress trajectories and plate convergence: earlier model from Angelier et al. (1986). (a) First compressional event. (b) Second compressional event. Philippine Sea plate hatchured, Eurasia white. Convergent boundary of eastern Taiwan with triangles on the upper side. Large arrows indicate relative motion Philippine Sea plate–Eurasia (azimuth between parentheses; see remarks in text). Trajectories of σ_1 with average deviation from the direction of plate convergence, in degrees (+ = clockwise; − = counter-clockwise). Dashed lines in (a) represent distribution of σ_1 paleostress trajectories in northernmost Taiwan (due to clockwise rotation of the area, confirmed later by Lee et al., 1991). Compare with models presented herein.

It is important to observe that the direction of plate convergence adopted in all the figures (except Figs. 8 and 9) was not adjusted in order to satisfy palaeostress distribution requirements, but imposed according to the independent kinematics information of Table 1. Also, as pointed out earlier, the influence of changes in rheological parameters plays a significant but moderate role. As a consequence, the general consistency between the stress distribution computed in the model and that observed based on onland field analyses, should not be considered artificial. The existence of a small but systematic misfit has been discussed and explained in an earlier section of this paper.

8. Conclusion

Based on previous experiments, we conclude that the distributions of stress trajectories in the Taiwan area are mainly controlled by: (1) the plate motion of the Philippine Sea plate relative to Eurasia; (2) the opening of the Okinawa Trough; (3) the geometric configuration of the boundary between the Eurasian continental margin and the Philippine Sea plate; and (4) the rheological properties of the model. These factors are summarized in Fig. 10a and Table 3. The study of a two-dimensional elastic and elasto–plastic finite-element modelling of the subduction–collision in and around Taiwan allows us to estimate the influences of these different parameters in the stress pattern. Taking into account both the simplifying assumptions of the numerical modelling and the angular uncertainties of field determinations, the fit between the calculated stress pattern of the finite-element model and that determined based on the geometrical synthesis of field analyses is rather good in general, so that our model is valid as a first approximation.

The results, mainly summarized in Figs. 10b and 11 and Table 4, are constrained by the actual distribution of the recent and present stress (Fig. 4). We have shown that although the direction of convergence plays a significant role, the shape of the plate boundary in the main factor controlling the fan-shaped trend distribution of the maximum compressional stress.

The asymmetric distribution of stress trajectories in Taiwan (Fig. 4b) is due to the geometry of the plate boundary (especially, the presence of the sharp northwestern corner of the Philippine Sea plate) and to the oblique collision of the Philippine Sea plate. The distribution of the stress trajectories is of course strongly influenced by the shape of the collision indenter, but the existence and velocity of a significant southward displacement of the Ryukyu Trench relative to Eurasia exerts a major influence on the stress distribution in northern Taiwan (Table 4, Figs. 10b and 13b).

We obtained a very limited rotation of this stress field through a large rotation of the direction of convergence (less than 1/3, see Fig. 8 and Table 5). We concluded, from this relative stability, that the stress pattern is principally dependent on the configuration of the plate boundaries. To this respect, the counterclockwise rotation of about 35° of the direction of convergence inferred from a similar rotation of the average trends of compression (Angelier et al., 1986; Fig. 14 and Table 6) may be exaggerated, and the changes in the shape of the collision zone should be more carefully considered in the analysis of stress-kinematics relationships through time.

Acknowledgements

Supports of this work were provided by the cooperation of I.F.T.-N.C.S. framework ('Institut Français à Taipei' and National Science Council of Taiwan), the French C.R.O.U.S. in Paris, the Ministry of Education of Taiwan. Collaboration partly supported by the Central Geological Survey of Taiwan, the P.N.T.S. program of the French C.N.R.S., and the National Taiwan University, allowed control by field data. We thank S. Manoussis for assistance in setting up the numerical modelling code, critical comments and suggestions by Drs F. Beekman and anonymous referees were very useful and enable us to improve the manuscript.

References

Angelier, J., 1979. Determination of the mean principal direction of stress for a given fault population. Tectonophysics, 56: T17–T26.

Angelier, J., 1984. Tectonic analysis of fault slip data sets. J. Geophys. Res., 89: 5835–5848.

Angelier, J., 1986. Preface — Geodynamic of the Eurasia–Philippine Sea plate boundary. Tectonophysics, 125: IX–X.

Angelier, J., 1990. Foreword — Geodynamics of the Eastern Eurasian Margin. Tectonophysics, 183: VII–X.

Angelier, J., Bergerat, F. and Chu, H.T., 1986. Plate collision and paleostress trajectories in a fold-and-thrust belt: the Foothills of Taiwan. Tectonophysics, 125: 161–178.

Angelier, J., Bergerat, F., Chu, H.T. and Lee, T.Q., 1990. Tectonic analysis and the evolution of a curved collision belt: the Hsüehshan Range, northern Taiwan. Tectonophysics, 183: 77–96.

Angelier, J., Lee, J.C. and Hu, J.C., 1994. Construction of trajectory maps based on local paleostress determinations and their interpretation: some new insights. In: F. Roure (Editor), Peri-Tethyan Platforms. Technip, Paris, pp. 129–144.

Barrier, E. 1985. Tectonique d'une chaîne de collision active: Taiwan. Mém. Sci. Terre, Univ. P. et M. Curie, Paris, 85-29, 492 pp.

Barrier, E., 1986. The double collision of Taiwan: an active orogen. Tectonophysics, 125: 39–72.

Barrier, E. and Angelier, J., 1986. Active collision in eastern Taiwan: the Coastal Range. Tectonophysics, 125: 39–72.

Biq, C.C., 1966. Tectonic styles and structural levels in Taiwan. Proc. Geol. Soc., 9: 3–9.

Bott, M.H.P., 1990. Stress distribution and plate boundary force associated with collision mountain ranges. Tectonophysics, 182: 193–209.

Bott, M.H.P., 1991. Sublithospheric loading and plate-boundary forces. Philos. Trans. R. Soc. London, A, 337: 83–93.

Chen, C.H. and Chu, H.T. 1983. The metamorphic facies map of Taiwan. Cent. Geol. Surv., Taipei, Taiwan, R.O.C.

Chen, C.H., Chu, H.T., Liou, J.G. and Ernst, W.G., 1983. Explanatory notes for the metamorphic facies map of Taiwan. Spec. Publ. Cent. Geol. Surv., Taipei, Taiwan, R.O.C., 2, 32 pp.

Chen, W.I. and Molnar, P., 1983. Focal depths of intracontinental and intraplate earthquakes and their implications for the thermal and mechanical properties of the lithosphere. J. Geophys. Res., 88: 4183–4214.

Chu, H.T., 1990. Néotectonique cassante et collision plio-quaternaire à Taiwan. Unpublished Ph.D. Thesis, Université Pierre et Marie Curie, Paris, 292 pp.

Chu, J.J., 1993. Paleostress analysis along the Hsin-Chung Fault (in Chinese). Unpublished Master Thesis, National Taiwan University, Taipei, Taiwan.

Delcaillau, B., Angelier, J. Herail, G., Chu, H.T., Lee, J.C., Liew, P M. Lin, T.S., Lu, C.Y., Teng, L. Deramond, J. and Souquet, P., 1993. Evolution morphostructurale et sédimentaire d'un bassin d'avant-pays en régime de collision oblique: le Piémont occidental de Taiwan. C.R. Acad. Sci. Paris, 315, Série II: 1239–11244.

DeMets, C.R., Gordon, R.G., Argus, D. and Stein, S., 1990. Current plate motions. Geophys. J. Int., 101: 425–478.

England, P. and Houseman, G., 1989. Extension during continental convergence, with application to the Tibetan Plateau. J. Geophys. Res., 94: B17,561–B17,579.

England, P. and Molnar, P., 1991. Inferences of deviatoric stress in actively deforming belts from simple physical models. Philos. Trans. R. Soc. London, A, 337: 151–164.

England, P. and Wortel, R., 1980. Some consequences of the subduction of young slabs. Earth Planet. Sci. Lett., 47: 403–415.

George, P.L., Laug, P., Muller, B. and Vidrascu, M., 1986. Guide d'utilisation et normes de programmation. 1, Inst. National Recherche Informatique Automatique, Le Chesnay, 113 pp.

Gough, D.I. and Gough, W.I., 1987. Stress near the surface of the earth. Annu. Rev. Earth Planet. Sci., 15: 545–566.

Ho, C.S., 1982. Tectonic evolution of Taiwan: explanatory text of the tectonic map of Taiwan. Ministry of Economic Affairs, Taiwan, R.O.C., 126 pp.

Ho, C.S., 1986. A synthesis of the geologic evolution of Taiwan. Tectonophysics, 125: 1–16.

Ho, C.S., 1988. An Introduction to the Geology of Taiwan: Explanatory Text of the Geologic Map of Taiwan. MOEA, 2nd ed., 192 pp.

Hsu, T.L., 1956. Geology of the Coastal Range, eastern Taiwan. Bull. Geol. Surv. Taiwan, 8: 39–64.

Hsu, T.L., 1962. Recent faulting in the Longitudinal Valley of eastern Taiwan. Mem. Geol. Soc. China, 1: 95–102.

Hsu, T.L., 1976. Neotectonics of the Longitudinal Valley, eastern Taiwan. Bull. Geol. Surv. Taiwan, 25: 53–62.

Huchon, P., 1986. Comment on 'Kinematics of the Philippine Sea plate' by B. Ranken, R.K. Cardwell and D.E. Karig. Tectonics, 1: 165–168.

Huchon, P., Barrier, E., De Bremaecker, J.C. and Angelier, J., 1986. Collision and stress trajectories in Taiwan: a finite element model. Tectonophysics, 125: 179–191.

Jahn, B.M., Martineau, F., Peucat, J. and Cornichet, J., 1986. Geochronology of the Tananao Schist Complex and crustal evolution of Taiwan. Mem. Geol. Soc. China, 7: 406–416.

Kimura, M., 1985. Back-arc rifting in the Okinawa Trough. Mar. Pet. Geol., 2: 222–240.

Lacombe, O., Angelier, J. and Laurent, P., 1993. Les macles de la calcite, marquers des compressions récentes dans un orogène actif : l'exemple des calcaires récifaux du Sud de Taiwan. C.R. Acad. Sci. Paris, 316, Série II: 1805–1813.

Lee, C.T., 1986. Methods of stress analysis and paleostress changes in northern Taiwan due to arc–continent collision (in Chinese). Unpublished Ph. D. thesis, National Taiwan University, Taipei, 370 pp.

Lee, J.C. and Angelier, J., 1993. Localisation des déformations actives et traitements des données géodésiques: l'example de la faille de la Vallée Longitudinale, Taïwan. Bull. Soc. Géol. Fr., 164, 4: 533–570.

Lee, J.C. and Angelier, J., 1994. Paleostress trajectories maps based on the results of local determinations: the 'lissage' program. Comput. Geosci., 20(2): 161–191.

Lee, T.Q., Angelier, J., Chu, H.T. and Bergerat, F., 1991. Rotations in the northern eastern collision belt of Taiwan: preliminary results from paleomagnetism. Tectonophysics, 199: 109–120.

Letouzey, J. and Kimura, M., 1985. The Okinawa Trough genesis, structure and evolution of a back-arc basin developed in a continent. Mar. Pet. Geol., 2: 111–130.

Letouzey, J. and Kimura, M., 1986. The Okinawa Trough: genesis of a back-arc basin developing along a continental margin. Tectonophysics, 125: 209–230.

Liou, J.G. and Ernst, W.G., 1984. Summary of Phanerozoic metamorphism in Taiwan. Mem. Geol. Soc. China, 6: 133–152.

Lu, C.Y. and Hsü, K.J., 1992. Tectonic evolution of the Taiwan Mountain Belt. Pet. Geol. Taiwan, 29: 15–35.

Lue, Y.T., Lee, T.Q., Horng, C.S. and Wong, Y., 1991. Magnetic fabric in the non-metamophosed terrain of the northwestern Foothills–Hsüehshan belts of Taiwan. Proc. Geol. Soc. China, 34: 131–146.

Mandl, G., 1988. Mechanics of Tectonic Faulting, Models and Basic Concepts. Elsevier, Amsterdam.

Minster, J.B. and Jordan, T.H., 1979. Rotation vectors for the Philippine and Rivera plates. EOS, Trans Am. Geophys. Union, 60: 958.

Mount, V.S. and Suppe, J., 1992. Present-day stress orientation adjacent to active strike-slip faults: California and Sumatra. J. Geophys. Res., 97: B11,955–B12,013.

Pelletier, B. and Stephan, J.F., 1986. Middle Miocene obduction and late Miocene beginning of collision registered in the Hengchun peninsula: geodynamic implications for the evolution of Taiwan. Tectonophysics, 125: 133–160.

Peltzer, G., 1988. Centrifuged experiments of continental scale tectonics in Asia. Acta Univ. Upsaliensis, 14: 115–128.

Ranalli, G. and Murphy, D., 1987. Rheological stratification of the lithosphere. Tectonophysics, 132: 281–295.

Ranken, B., Cardwell, R.K. and Karig, D.E., 1984. Kinematics of the Philippine Sea Plate. Tectonics, 3: 555–575.

Roecker, S.W., Yeh, Y.H. and Tsai, Y.B., 1987. Three dimensional P and S wave velocity structure beneath Taiwan. J. Geophys. Res., 92: B10,547–B10,570.

Seno, T., 1977. The instantaneous rotation vector of the Philippine Sea plate relative to the Eurasian plate. Tectonophysics, 42: 209–226.

Seno, T., Moriyama, T., Stein, S., Woods, D.F., Demets, C., Argus, D. and Gordon, R., 1987. Redetermination of the Philippine Sea plate motion. EOS, Trans Am. Geophys. Union, 68: 1474.

Seno, T., Stein S. and Gripp, A.E., 1993. A model for the motion of the Philippine Sea plate consistent with NUVEL-1 and geological data. J. Geophys. Res., 98: B17,941–B17,948.

Sibuet, J.C., Letouzey, J., Barbier, F., Charvet, J., Foucher, J.P., Hilde, Thomas W.C., Kimura, M., Chiao, L.Y., Marsset, B.,

Muller, C. and Stephan, J.F., 1987. Back arc extension in the Okinawa Trough. J. Geophys. Res., 92: 14,041–14,063.

Suppe, J., 1980. A retrodeformable section of northern Taiwan. Proc. Geol. Soc. China, 23: 46–55.

Suppe, J., 1981. Mechanics of mountain building and metamorphism in Taiwan. Mem. Geol. Soc. China, 4: 67–89.

Suppe, J., 1984. Kinematics of arc–continent collision, flipping of subduction, and back-arc spreading near Taiwan. Mem. Geol. Soc. China, 6: 21–33.

Suppe, J., Hu, C.T. and Chen, Y.J., 1985. Present-day stress direction in western Taiwan inferred from borehole elongation. Pet. Geol. Taiwan, 21: 1–12.

Tapponnier, P., Peltzer, G., Le Dain, A.Y., Armijo, R. and Cobbold, P., 1982. Propagating extrusion tectonics in Asia: new insights from simple experiments with plasticine. Geology, 10: 611–616.

Teng, L.S., 1990. Geotectonic evolution of late Cenozoic arc–continent collision in Taiwan. Tectonophysics, 183: 57–76.

Teng, L.S., Chen, C.H., Wang, W.S., Liu, T.K., Jung, W.S. and Chen, J.C., 1992. Plate kinematic model for Late Cenozoic arc magmatism in northern Taiwan. J. Geol. Soc. China, 35: 1–18.

Tsai, Y.B., 1986. Seismotectonics of Taiwan. Tectonophysics, 125: 17–37.

Tsai, Y.B., Teng, T.L., Chiu, J.M. and Liu, H.L., 1977. Tectonic implications of the seismicity in the Taiwan region. Mem. Geol. Soc. China, 2: 13–41.

Viallon, C., Huchon, P. and Barrier, E., 1986. Opening of the Okinawa basin and collision in Taiwan: a retreating trench model with lateral anchoring. Earth Planet. Sci. Lett., 80: 145–155.

Vilotte, J.P., Daignières, M. and Madariaga, R., 1982. Numerical modeling of intraplate deformation: simple mechanical models of continental collision. J. Geophys. Res., 87: B10,709–B10,728.

Wortel, M.J.R. and Cloetingh, S.A.P.L., 1985. Accretion and lateral variations in tectonic structure along the Peru–Chile trench. Tectonophysics, 112: 443–462.

Wortel, M.J.R., Remkes, M.J.N., Govers, R., Cloetingh, S.A.P.L. and Meijer, P.Th., 1991. Dynamics of the lithosphere and the intraplate stress field. Philos. Trans. R. London, A, 337: 111–126.

Wu, F.T., 1978. Recent tectonics in Taiwan. J. Phys. Earth, 26: S265–S299.

Yeh, Y.H., Lin, C.H. and Roecker, S.W., 1989. A study of upper crustal structures beneath northeastern Taiwan: possible evidence of the western extension of Okinawa Trough. Proc. Geol. Soc. China, 32(2): 139–156.

Yeh, Y.H., Barrier, E., Lin, C.H. and Angelier, J., 1991. Stress tensor analysis in the Taiwan area from focal mechanisms of earthquakes. Tectonophysics, 200: 276–280.

Yen, T.P., 1973. Plate tectonics in the Taiwan Range. Proc. Geol. Soc. China, 16: 7–23.

Yu, S.B. and Kuo, L.C., 1994. Utilizing continuous GPS observed data to study the crustal deformation in Taiwan (abstr.). Annu. Meet. Geol. Soc. China.

Yu, S.B. and Liu, C.C., 1989. Fault creep on the central segment of the Longitudinal Fault, eastern Taiwan. Proc. Geol. Soc. China, 32(3): 209–231.